# Modeling ionospheric TEC using gradient boosting based and stacking machine learning techniques

**Ayanew Nigusie[1,2,*], Ambelu Tebabal[1], and Roman Galas[3]**

[1]Department of Physics, Washera Geospace and Radar Science Research Laboratory, Bahir Dar University, Bahir Dar, Ethiopia

[2]Department of Physics, Oda Bultum University, Chiro, Ethiopia

[3]Department of Geodesy and Geoinformation Science, Chair of Precision Navigation and -Positioning, Technical University of Berlin, Berlin, Germany

**Key Points:**

- Three gradient-boosting decision tree-based algorithms and their stacked combination with the linear regression algorithm are applied.
- The predictions of the machine learning models are strongly correlated with the GPS VTEC, with a correlation coefficient of ∼0.96.
- The machine learning models utilized in this work significantly outperformed the International Reference Ionosphere (IRI 2020) global model.

Corresponding author: A. Nigusie, ayanew.nigusie@gmail.com

## Abstract

Accurately predicting and modeling the total electron content (TEC) of the ionosphere can greatly improve the accuracy of satellite navigation and positioning and help to correct ionospheric delay. This study tested the effectiveness of four different machine learning (ML) models in predicting hourly vertical TEC (VTEC) data from a single station in Addis Ababa, Ethiopia. The models used were gradient boosting machine (GBM), extreme gradient boosting (XGBoost), light gradient boosting machine (LightGBM) algorithms, and a stacked combination of these algorithms with a linear regression algorithm. The models relied on input variables that represent solar activity, geomagnetic activity, season, time of the day, interplanetary magnetic field, and solar wind. The models were trained using the VTEC data from January 2011 to December 2018, excluding the testing data. The testing data comprised the data for the year 2015 and the initial six months of 2017. The RandomizedSearchCV algorithm was used to determine the optimal hyperparameters of the models. The predicted VTEC values of the four ML models were strongly correlated with the GPS VTEC, with a correlation coefficient of $\sim$0.96, which is significantly higher than the corresponding value of the International Reference Ionosphere (IRI 2020) model, which is 0.87. Comparing the GPS VTEC values with the predicted VTEC values based on diurnal and seasonal characteristics showed that the predictions of the developed models were generally in good agreement and outperformed the IRI 2020 model. Overall, the GBDT-based algorithms and their stacked integration demonstrated promising potential for predicting VTEC over Addis Ababa, Ethiopia.


## Plain Language Summary

Studying the ionosphere is crucial as it significantly impacts satellite navigation and communication systems. However, a major challenge in ionospheric studies is the unavailability of observational TEC data in some regions. To tackle this problem, researchers have employed machine learning modeling as a solution. In this study, we used machine learning algorithms such as gradient boosting machine, XGBoost, and LightGBM, as well as their stacked integration along with the linear regression algorithm, to model the ionospheric vertical total electron content over a single GPS receiver station in the low-latitude ionospheric region. The methods employed are highly efficient in terms of computational resources.

## 1 Introduction

The ionosphere, which is the upper portion of Earth's atmosphere, comprises ionized plasma that undergoes variations in its composition due to factors such as latitude and longitude, local time, season, solar and geomagnetic activity, and other factors. The electromagnetic wave propagating through this dynamic environment suffers a range delay whose magnitude depends on the frequency of the wave and the amount of the total electron content (TEC) (Shi et al., 2022; Hajra et al., 2016). TEC, which is the total number of electrons within a unit-square-meter column along a path through the ionopsphere, is a significant parameter characterizing ionospheric variability (Tang et al., 2022). For long-range radio communications, surveying, navigation, and other space weather-related operations, it is necessary to understand the changes in TEC.

Over the years, to better understand and mitigate the effect of ionospheric delay, the ionospheric community and others have investigated the ionospheric delay error in trans-ionospheric signals (Davies & Hartmann, 1997; Liu et al., 2020). There are, however, challenges associated with ionospheric studies due to the lack of observational data on the necessary time and spatial scales. This led to the development of global ionospheric models like NeQuick (Hochegger et al., 2000; Nava et al., 2008) and International Reference Ionosphere (IRI) models (Bilitza, 2001; Bilitza et al., 2011, 2017) . Despite their ability to improve several aspects of ionospheric modeling, different research findings (e.g., Nigussie et al., 2013; Okoh et al., 2018; Tebabal et al., 2018; Habarulema et al., 2007, 2009) have highlighted the shortcomings of these global models in the African sector. Several neural network (NN)-based single station and regional models have been developed in the African region to fill these gaps and improve prediction accuracy (e.g., Tebabal et al., 2018, 2019; Habarulema et al., 2007, 2009, 2011; Okoh et al., 2016, 2018; Habyarimana et al., 2020). It was found from these studies that NN-based models are very promising at capturing the overall dynamics of ionospheric variations compared to global models. However, this does not imply that the NN models always provide accurate predictions in all cases as compared to other machine learning techniques. NN algorithms tend to overfit small datasets due to their need for large amounts of data to fully exploit their potential (Natras et al., 2022).

In recent years, gradient-boosting decision tree (GBDT)-based machine learning techniques like extreme gradient boosting (XGBoost) (Chen & Guestrin, 2016) and light

gradient boosting machine (LightGBM) (Ke et al., 2017) have been created. These methods have been successfully used for modeling and forecasting of ionospheric TEC (e.g., Natras et al., 2022; Zhukov et al., 2021; Han et al., 2021). The findings have demonstrated that GBDT techniques are efficient and accurate in ionospheric modeling. Thus, adopting GBDT algorithms for ionospheric modeling is efficient in regions where there is a shortage of ionospheric TEC data, as these techniques are effective for both small and large datasets. Apart from that, GBDT-based algorithms are not expensive because they don't necessitate a significant amount of computational resources and training time compared to NN algorithms (Bentéjac et al., 2021). As a result, GBDT algorithms are relatively simple to optimize compared to NN techniques.

In previous studies conducted in the African region, machine learning methodologies other than GBDT-based algorithms were primarily used for modeling ionospheric vertical TEC (VTEC). Therefore, this study has been conducted to test the effectiveness of GBDT-based algorithms and their stacked integration to model VTEC. For this purpose, gradient boosting machine (GBM), XGBoost, LightGBM, and a stacked model of these three algorithms with a linear regression model are employed at a single GPS station over Addis Ababa, Ethiopia. Additionally, the present study has incorporated model input parameters that represent the influence of the interplanetary magnetic field (IMF) and solar wind, which have not been utilized in prior neural network-based models in the African region. In order to validate their predictive capability, the performances of the machine learning models used in this study are also assessed by comparing them with the International Reference Ionosphere (IRI 2020) global ionospheric model.

## 2 Data and Methods

### 2.1 Data and Data Preparation

The hourly VTEC data was obtained from a dual-frequency GPS receiver located over Addis Ababa, Ethiopia (ADIS, with geo lat: 9.0351° N and geo long: 38.7663° E). The values were derived using the calibration technique of Ciraolo et al. (2007) from 2011 through 2018. This data is publicly available at the Global Navigation Satellite System (GNSS) TEC calibration service provided by the International Center for Theoretical Physics (ICTP). To mitigate errors caused by multipath effects, only VTEC values ob-

tained at elevation mask angles greater than 30° were considered. The calibrated VTEC data sampling was 30-second and was then averaged to hourly values.

The fundamental principle used to obtain ionospheric TEC values from GPS observations is that GPS signals with varying frequencies encounter distinct ionosphere time delays as they pass through the same part of the ionosphere. A GPS signal with frequency $f$ will experience an ionospheric time delay $t$, which can be given by Klobuchar (1996) as:

$$t = 40.3\frac{TEC}{cf^2} \tag{1}$$

where c is the speed of light in free space. Dual-frequency GPS receivers make use of two frequencies, L1 (1575.42 MHz) and L2 (1227.60 MHz), in order to compensate for the delay caused by the ionosphere. This particular receiver, operating at frequencies $f_1$ and $f_2$, calculates the discrepancy in time delay between the two frequencies, given by

$$\Delta t = 40.3\frac{TEC}{c(f_2^2 - f_1^2)} \tag{2}$$

Therefore, the measured time delay ($\Delta$t) between the L1 and L2 frequencies is utilized for the computation of the TEC along the path of the ray. The slant TEC (STEC) measurements made here are the sum of the actual slant TEC, the GPS satellite differential delay $b_S$ (satellite bias), and the receiver differential delay $b_R$ (receiver bias). Thus, the VTEC can be given by (Rama Rao et al., 2006; Ciraolo et al., 2007)

$$VTEC = \frac{(STEC - (b_R + b_S))}{S(\varepsilon)} \tag{3}$$

where S($\varepsilon$) is the obliquity factor (mapping function) with zenith angle, $\theta_z$ at the ionospheric pierce point, defined by (Mannucci et al., 1993; Rama Rao et al., 2006)

$$S(\varepsilon) = \frac{1}{\cos(\theta_z)} = \left\{1 - \left(\frac{R_E \times \cos(\varepsilon)}{R_E + h_S}\right)^2\right\}^{-0.5} \tag{4}$$

where $R_E$ is the mean radius of the Earth in km, $h_S$ is the height of the ionospheric pierce point, and $\varepsilon$ is the elevation angle in degrees.

The variability of VTEC is modeled as a function of known physical and geophysical parameters. Several of these factors have been well documented, including solar and geomagnetic activity, seasonal changes, and diurnal variations (e.g. Maruyama, 2007; Habarulema et al., 2007, 2009; Tebabal et al., 2018, 2019). The variation associated with season and time of the day is effectively represented by the day number of the year (DOY) and the

hour of the day (HR), respectively. The measure of solar activity is represented by the sunspot number and the 28- and 81-day moving averages of solar radio flux at 10.7 cm wavelength (F10.7 index). The planetary amplitude (ap index) and the disturbance storm time (Dst index) were used as inputs for geomagnetic activity. The solar wind plasma speed (SW) and the north-south component of the interplanetary magnetic field (IMF Bz) based on the Geocentric Solar Ecliptic System (GSE) were also used as input variables. The data for the input variables was obtained from the Goddard Space Flight Center Space Physics Data Facility. The data for these input variables was downloaded at hourly intervals and used as external geophysical driving sources to improve the predictive performance of the models.

### 2.2 Modeling Techniques

This study utilized machine learning algorithms for the purpose of creating models. Machine learning allows computers to recognize patterns, make predictions, and make decisions by analyzing and adapting to data rather than relying on explicit instructions (Zhou, 2021). Ensemble learning, a technique that combines multiple models to solve computational problems and enhance prediction accuracy, is employed. Bagging, boosting, and stacking are the most commonly used ensemble machine learning algorithms, and this study used models based on boosting and stacking methodologies (Sagi & Rokach, 2018; Yang, 2017). Boosting is a technique that improves the predictions of weak learners by adding them sequentially. This involves training a new weak learner model based on the errors of the previously learned models (Natekin & Knoll, 2013). In tree-boosting ensembles, decision trees are often used as weak learners. Decision trees are supervised learning techniques that can be used for tasks like classification and regression. In regression trees, the goal is to make predictions of continuous values, and the accuracy of these predictions is assessed by calculating the sum of squared differences between the predicted values and the actual values (Hastie et al., 2009; Rokach & Maimon, 2005). Gradient tree boosting is a boosting ensemble technique that uses a combination of decision trees and an additive model to minimize a loss function (Brownlee, 2016).

#### *2.2.1 Gradient Boosting Machine (GBM)*

A gradient-boosting machine uses a learning method that fits new models in succession to improve the accuracy of the response variable estimation. The GBM algorithm

aims to construct predictive models using back-fitting and non-parametric regressions. Rather than creating just one model, the GBM begins by generating an initial model and continuously adjusts new models by minimizing the loss function to achieve the most accurate model (He et al., 2019). The algorithm's main concept is to create new base learners that are highly correlated with the negative gradient of the loss function and associated with the entire ensemble. The loss functions used can be any differentiable functions, but to provide a clearer understanding, if the error function is the classic squared-error loss, the training process will lead to successive fitting of errors (Natekin & Knoll, 2013).

#### *2.2.2 Extreme Gradient Boosting (XGBoost)*

XGBoost is a scalable and enhanced implementation of gradient-boosted decision trees. XGBoost is an open-source library that was initially developed by Tianqi Chen in 2014 and now has contributions from many developers. XGBoost is highly scalable because of various system and algorithmic optimizations. These include a unique tree learning algorithm for sparse data, a weighted quantile sketch procedure for handling instance weights, and parallel computing for faster learning. XGBoost also allows data scientists to process large amounts of data on a desktop using out-of-core computation (Brownlee, 2016; Chen & Guestrin, 2016). XGBoost uses a term called objective function, which is the sum of the loss function and a regularization term. This term plays a crucial role in reducing overfitting by promoting smoother learning of weights. Like GBM, XGBoost constructs a successive extension of the objective function through the reduction of a loss function. XGBoost uses Taylor expansion of the loss function up to the second order to discover the best solution, which is then used to balance the complexity of the model and the decline of the objective function in order to prevent overfitting (Fafalios et al., 2020).

#### *2.2.3 Light Gradient Boosting Machine (LightGBM)*

LightGBM is a high-performing implementation of the gradient-boosting decision tree algorithm developed by Microsoft in 2017. It is designed to handle large datasets and improve prediction accuracy. It does this by using a leaf-wise tree growth approach, which focuses on nodes with the highest change in loss. Additionally, it incorporates techniques such as gradient-based one-side sampling (GOSS) and exclusive feature bundling (EFB) to enhance efficiency. The GOSS method selectively keeps instances with large

gradients and drops instances with small gradients to better estimate information gain. This approach is more effective than random sampling, particularly when the range of information gained is wide. In sparse, high-dimensional data, features that do not occur together can be combined into one feature bundle to reduce the number of features using the EFB technique (Ke et al., 2017).

#### *2.2.4 Stacking Ensemble Technique*

A stacking technique is a type of ensemble machine learning algorithm that uses meta-learning techniques to find the best way to combine predictions from multiple base models. It involves two stages: training the base models and training the meta model. In the first stage, the original data is split into a training set and a testing set, and the training set is trained using k-fold cross-validation. In the second stage, the predictions from the base models are reassembled in the original order and used to create a new training set for the meta model. The predictions from the testing sets of the base models are combined to form the testing set for the meta model. Finally, the meta model is trained using this new dataset (Lu et al., 2023). In this study we have applied stacking ensemble learning, using the linear regression (LR), GBM, XGBoost, and LightGBM as the base models and the LR as the a final meta model. Linear regression is a modeling technique that linearly combine explanatory variables to predict a response variable (Hastie et al., 2009).

### 2.3 Development of the Models

We have used 8-year (2011–2018) GPS VTEC data at an hourly interval at ADIS GPS station to train and test the models. Missing data is very common in GNSS monitoring time series when collecting and processing raw data from GNSS stations. As a result, there are a significant number of missing VTEC values at the ADIS GPS station. Therefore, to fill these gaps, the nearby GPS stations VTEC data from ABOO (8.99° N, 37.81°E) and NAZR (8.57°N, 39.29°E) was utilized. Selecting appropriate inputs is crucial for designing an effective machine-learning model. It determines the model's ability to learn and generalize the relationship between the inputs and the target. In order to align the input variables with the VTEC, an approximation function can be used. This function establishes a nonlinear connection between the input data and the VTEC prediction output based on the input variables. As the function is not known, it is estimated

by optimizing the machine learning algorithms for the purpose of VTEC prediction, as explained by Hastie et al. (2009). The testing data used to assess model performance consisted of data for the year 2015 and the first six months of 2017, which represented 20% of the total data. The remaining data was used to train the models and estimate the optimal parameters. The steps we followed to develop the machine learning models are shown in Figure 1.

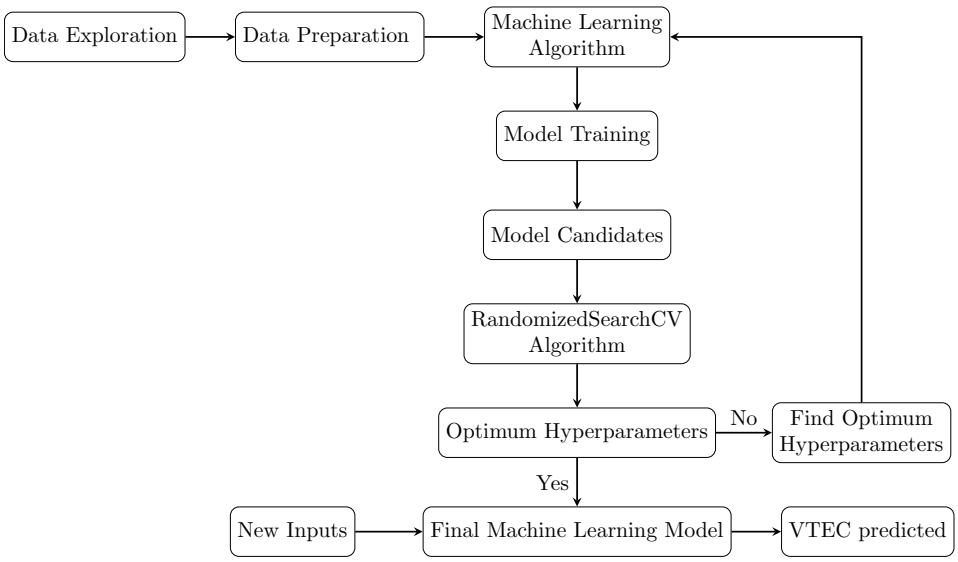


**Figure 1.** Diagram of the development of the VTEC machine learning models

### *2.3.1 Model Optimization*

Machine learning algorithms contain a set of parameters, called hyperparameters, that cannot be predicted from data and must instead be customized for a particular learning problem. Hyperparameters specify the complexity and construction of the model. Depending on the data and the problem, the optimal values of hyperparameters may differ, and they are often discovered by testing with varying combinations and analyzing how well each model performs. Hyperparameters of boosting ensemble machine learning techniques that frequently require optimization include the maximum depth of the tree (max_depth), minimum loss reduction to create a new tree split (gamma), the number of trees used in ensemble learning (n_estimators), the fraction of samples to be used for fitting the individual base learners (subsample), the learning rate to reduce the gradient step (learning_rate), and the maximum number of leaves in each weak learner (num_leaves).

The RandomizedSearchCV algorithm was applied to the training data to determine the optimal hyperparameters for the three gradient boosting models used in this study. RandomizedSearchCV is an algorithm that combines random search with cross-validation to randomly select combinations of hyperparameters to train the model. Cross-validation is an approach to measuring the performance of a model by training it on a particular portion of input data and then testing it on a subset of input data that has not been used before (Rahmadayana et al., 2021). The selected optimal hyperparameters and the range of values used to search for the best hyperparameters are provided in Table 1.

| Model | Hyperparameters used | Range of Search |
|---|---|---|
| GBM | max_depth = 6 | (3,4,5,6,7,8,9,10,11,12,13,14,15) |
| | subsample = 1 | (0.1,0.2,0.3,0.4,0.5,0.6,0.7,0.8,0.9,1) |
| | learning_rate = 0.1 | (0.01,0.03,0.04,0.05,0.06,0.08,0.1, 0.15,0.2) |
| | n_estimators = 200 | (100,150,200,250,300,350,400,450,500,600) |
| XGBoost | max_depth = 6 | (3,4,5,6,7,8,9,10,11,12,13,14,15) |
| | learning_rate = 0.05 | (0.01,0.02,0.04,0.05,0.06,0.08,0.1,0.15,0.2) |
| | gamma = 0.5 | (0.1,0.2,0.3,0.4,0.5,0.6,0.7,0.8,1,1.1,1.2,1.3) |
| | n_estimators = 200 | (100,150,200,250,300,350,400,450,500,600) |
| LightGBM | max_depth = 5 | (3,4,5,6,7,8,10,11,12,13,14,15) |
| | num_leaves=300 | (100,200,250,300,350,400,450,500) |
| | learning_rate = 0.1 | (0.01,0.03,0.04,0.05,0.06,0.08,0.1,0.15,0.2) |
| | n_estimators = 300 | (100,150,200,250,300,350,400,450,500,600) |

**Table 1.** Hyperparameters used to build GBM, XGBoost, and LightGBM models.

### *2.3.2 Model Evaluation*

To evaluate the effectiveness of the models, we have utilized various statistical parameters such as residual error ($r_i$), root-mean-square error (RMSE), mean absolute error (MAE), standard deviation of residual errors ($\sigma$), and correlation coefficient (R). These parameters are widely recognized and utilized to determine the performance of a model(Shi

et al., 2022; Xiong et al., 2021). The equations are as follows:

$$
\begin{aligned}
r_i &= VTEC_i^{Obs} - VTEC_i^{Pred} \\
RMSE &= \sqrt{\frac{1}{N}\sum_{i=1}^{N}(VTEC_i^{Obs} - VTEC_i^{Pred})^2} \\
MAE &= \frac{1}{N}\sum_{i=1}^{N}|VTEC_i^{Obs} - VTEC_i^{Pred}| \\
\sigma &= \sqrt{\frac{\sum_{i=1}^{N}(r_i - \bar{r}_i)}{N-1}} \\
R &= \frac{\sum_{i=1}^{N}(VTEC_i^{Obs} - \overline{VTEC}^{Obs})(VTEC_i^{Pred} - \overline{VTEC}^{Pred})}{\sqrt{\sum_{i=1}^{N}(VTEC_i^{Obs} - \overline{VTEC}^{Obs})^2 \sum_{i=1}^{N}(VTEC_i^{Pred} - \overline{VTEC}^{Pred})^2}}
\end{aligned}
\tag{5}
$$

where N is the number of data points, $\text{VTEC}_i^{Obs}$ is the GPS VTEC value, $\text{VTEC}_i^{Pred}$ is the predicted VTEC value of the $i^{th}$ data point, $\overline{VTEC}^{Obs}$ is the mean of GPS VTEC values, $\overline{VTEC}^{Pred}$ is the mean of predicted VTEC, and $\bar{r}_i$ is the mean of the residuals for i = 1, 2,..., N.

## 3 Results and Discussion

### 3.1 Performance of the Models

We utilized gradient boosting and stacking machine learning techniques to investigate their effectiveness in VTEC modeling. The dataset for the years 2011–2014, 2016, 2018, and the second half of 2017 was used in developing the ML models. Once the establishment of the models was done, we saved the model hyperparameters for future applications. The data for 2015 and the first six months of 2017 was then used to test the models. The scatter plots of the predicted VTEC by each model against the GPS VTEC for the testing data are shown in Figure 2. The horizontal axis represents the observed values, while the vertical axis represents the predicted values. A scatter-fitted red-colored solid line is defined by $y = f(x)$, where y represents the predicted value and x represents the GPS VTEC value. As seen from the figure, it is evident that the modeled VTEC values have a strong correlation with the observational values of GPS VTEC, with a correlation coefficient of R $\approx$ 0.96. This high correlation indicates that the ML models can precisely represent most of the variations and are capable of explaining over 98% of the variability of GPS VTEC. To enable further comparisons, we present a contour plot in Figure 3 that highlights the differences in error distribution between GPS VTEC and

predicted values for the testing periods. The x-axis represents the DOY, while the y-axis represents universal time coordinates (UTC). The maximum differences between GPS VTEC and predicted VTEC by GBM, XGBoost, LightGBM, and Stacked models are 27.5, 28.0, 29.5, and 27.0 TECU, respectively. The LightGBM and Stacked models showed 72% and 75% of data points, respectively, with absolute residual errors within the range of 0 and 5 TECU. Meanwhile, both GBM and XGBoost models demonstrated 73% of data points. Therefore, it can be concluded that the stacked model is slightly better at reducing errors when compared to other gradient-boosting decision tree (GBDT)-based techniques.

Table 2 is a summary of the R, RMSE, MAE, and $\sigma$ values computed using GPS VTEC and modeled VTEC for both the ML models (from 4 algorithms) and the IRI 2020 model. The RMSE, MAE, and $\sigma$ values for ML models are considerably smaller than those obtained from the IRI 2020 global model, indicating superior performance. These statistical analysis confirms that ML models are well-trained with the training data and exhibit accurate predictions for new datasets. Although there is no significant difference between statistical values of the four ML models, the stacked ensemble model shows a slight improvement of $\sim$0.2 TECU in RMSE and $\sigma$ compared to individual GBDT-based models. To better display the ability of the GDBT models to reproduce the temporal feature of the VTEC, Figure 4 indicates the VTEC maps for high and low solar activity periods of years 2015 and 2017, respectively, for both GPS VTEC and modeled values. The accurate predictions of daily, seasonal, and annual VTEC variations are visible on the maps for model predictions in year 2015. However, in year 2017, the models tend to overestimate VTEC predictions at the beginning of April. This could be due to reliance on data from periods of high solar activity.

The results of the current study indicate that the performance level of the ML models developed is comparable to, or in most cases, better than, other existing single-station and regional models applied in the low-latitude African region. The models showed exceptional prediction accuracy with minimal error. The testing data produced an RMSE value of approximately 5.3 TECU for the three GBDT models, while the stacked model achieved an RMSE value of 5.1 TECU. In contrast, previous studies by Tebabal et al. (2018) on a single-station feed neural network-based model over Arba Minch, Ethiopia, yielded R and RMSE values of 0.95 and 6.0 TECU, respectively, which are less favorable than those obtained in our study. Similarly, in another single-station neural network-

based model over Mbarara, Uganda, by Habyarimana et al. (2020), an RMSE value of 5.7 TECU was found, which exceeded the RMSE values achieved in the present study. Okoh et al. (2016) reported that the RMSE values for a neural network-based model over Nigeria ranged from 5.4 to 12.6 TECU, which is significantly higher than the values obtained in our study. Another regional neural network-based model over Ethiopia, developed by Tebabal et al. (2019), reported RMSE values ranging from 3.8 to 6.5 TECU, which are comparable to the values obtained in this study.

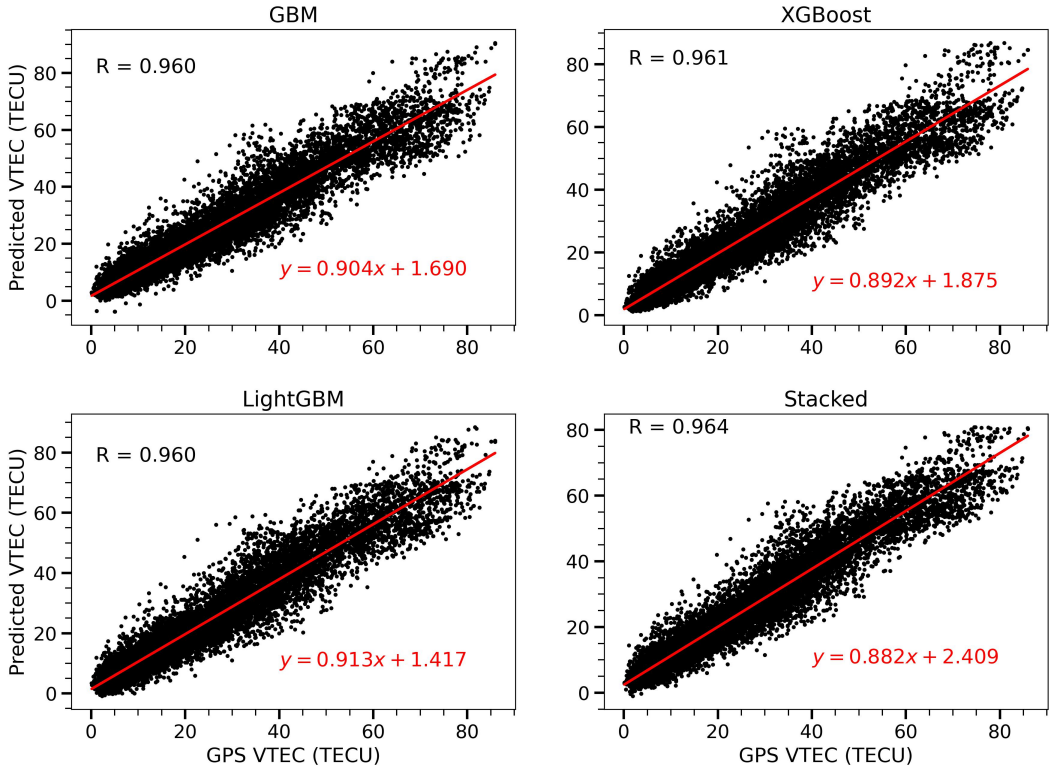


**Figure 2.** Scatter plots for hourly GPS VTEC and corresponding modeled VTEC values using different ML algorithms on the testing data

### 3.2 Day-to-day variability

In this section, the day-to-day variations between the observed and predicted VTEC values are presented. The performance of the models was tested on both quiet and disturbed days based on the unseen data. The quiet and disturbed days for the analysis were chosen based on the Dst-index values.

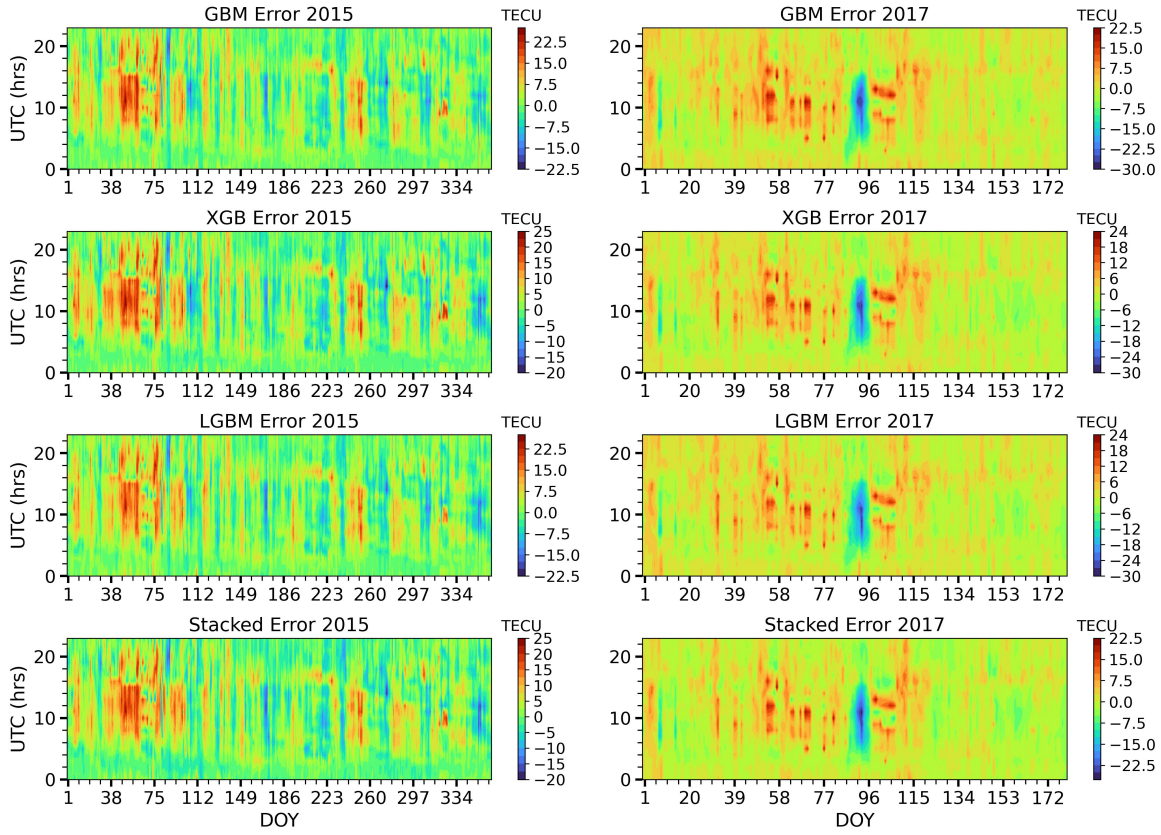


**Figure 3.** Contour plots of residual errors between the GPS VTEC and the VTEC predicted by the models for years 2015 (left panel) and 2017 (right panel).

| Models | R | RMSE (TECU) | MAE (TECU) | $\sigma$ (TECU) |
|---|---|---|---|---|
| GBM | 0.960 | 5.355 | 3.801 | 5.313 |
| XGBoost | 0.961 | 5.322 | 3.786 | 5.264 |
| LightGBM | 0.960 | 5.326 | 3.811 | 5.275 |
| Stacked | 0.964 | 5.143 | 3.717 | 5.120 |
| IRI 2020 | 0.873 | 11.782 | 8.117 | 10.956 |

**Table 2.** Table of R, RMSE, MAE, and $\sigma$ values of the machine learning models and IRI 2020 model for testing data.

#### *3.2.1 Quiet Time*

The performance of the models under geomagnetically undisturbed conditions was evaluated by comparing the predicted VTEC values with GPS VTEC and IRI 2020 model

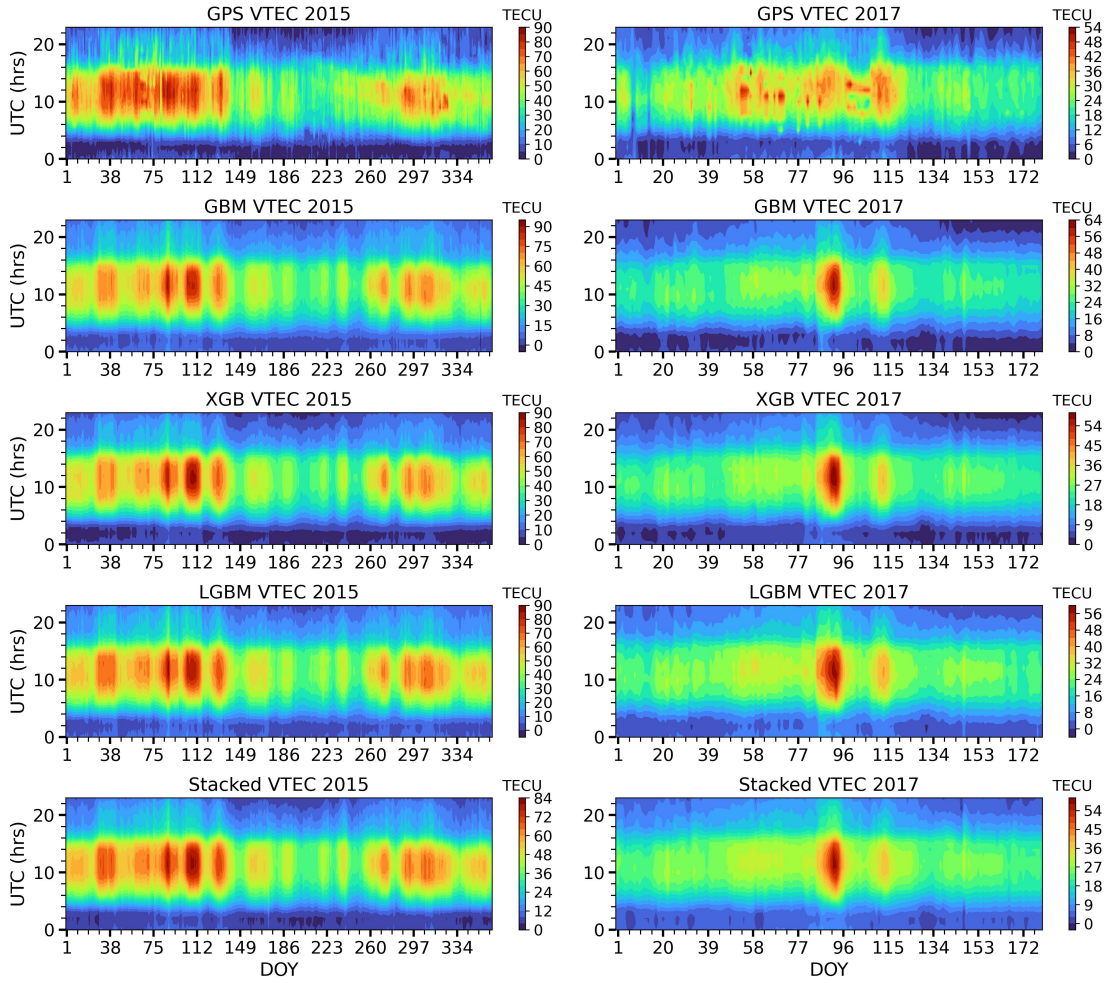


**Figure 4.** Contour plots of the GPS VTEC and the VTEC predicted by the models for years 2015 (left panel) and 2017 (right panel)

predictions on selected quiet days (-20 nT $\leq$ Dst $\leq$ -20 nT) in September and December 2015, and March and June 2017. Figure 5 shows the comparison for the quiet days of September 2015, December 2015, March 2017, and June 2017. In the figure, the red solid lines represent GPS VTEC, while the blue, black, lime (yellow-green), dark violet, and orange-colored lines depict VTEC values predicted by the GBM, XGBoost (XGB), LightGBM (LGBM), stacked (STK), and IRI 2020 models, respectively. The results suggest that the machine learning (ML) models consistently exhibit better agreement with GPS VTEC predictions on these selected quiet days. In each instance, the VTEC predictions by the ML models closely align with GPS VTEC, outperforming the IRI 2020 model, as shown in the plots for the quiet days.

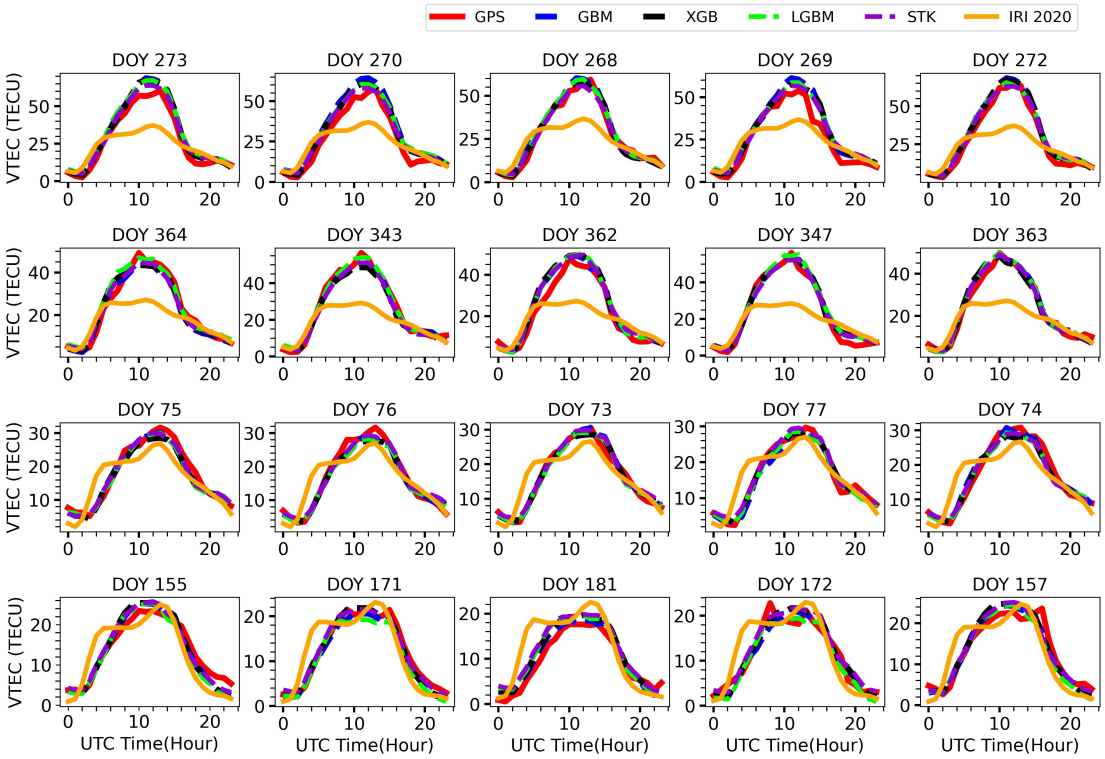


**Figure 5.** Comparison of predicted VTEC with the GPS VTEC for five quiet days of the months of September 2015 (first row), December 2015 (second row), March 2017 (third row), and June 2017 (fourth row).

### *3.2.2 Disturbed Conditions*

To assess how well the models can predict VTEC during geomagnetic disturbances, we compared the predicted VTEC values of the four ML and IRI 2020 models with the GPS VTEC. We analyzed the comparisons between predicted VTEC and GPS VTEC during intense (-200 nT<Dst≤-100 nT), moderate (-100 nT<Dst≤-50 nT), and weak (-50 nT<Dst≤-30 nT) geomagnetic storms. We selected three intense storm days on June 23, 2015 (minimum Dst = -198 nT), October 7, 2015 (minimum Dst = -130 nT), and May 28, 2017 (minimum Dst = -125 nT). Also, we chose three moderate storm days on September 20, 2015, April 16, 2015, and March 27, 2017, with minimum Dst values of -81, -88, and -70 nT, respectively. Moreover, we selected three weak storm days on January 26, 2015, October 1, 2015, and September 14, 2015, with minimum Dst values of -43, -40, and -47 nT, respectively. The figures in this report present the variations of the Dst index and comparisons of VTEC, which is predicted by machine learning and IRI

2020 models, with GPS VTEC for five-day periods during each event. The periods are centered on the day with the peak Dst index for intense, moderate, and weak geomagnetic storms. Figures 6, 7, and 8 show the results, respectively. In the graphs, GPS VTEC is shown with a red-colored solid line, and the VTEC values predicted by GBM, XGBoost (XGB), LightGBM (LGBM), stacked (STK), and IRI 2020 models are represented by blue, black, lime, dark violet, and orange-colored lines.

The plots show that the ML models effectively captured the variations in VTEC and were closely aligned with GPS VTEC measurements, unlike the IRI 2020 model, which had less accurate VTEC predictions in most instances. During the intense storm period from June 21–25, 2015, the ML models slightly overestimated GPS VTEC but were still well captured by the IRI 2020 model in the early stages of the storm. The ML models accurately predicted VTEC during the intense storm day and the subsequent recovery phase, while the IRI 2020 model underestimated it. During the intense storm period from October 7-9, 2015, the storm caused an enhancement in VTEC the following day; however, the models slightly underestimated the enhancement in GPS VTEC. This may be because the models may not have obtained the necessary information from the training data to make predictions during such times since all geomagnetic storms don't result in VTEC enhancements. The bar graph in Figure 9 compares the RMSE values of the four ML models with the IRI 2020 model for selected geomagnetic storm periods. This comparison aims to evaluate the performance of the models during geomagnetic disturbances. The RMSE values of all ML models are consistently much lower than the RMSE values of the IRI 2020 model during every geomagnetic storm period. During five of the chosen storm periods, the stacked model shows slightly lower RMSE values than the three GBDT models. This suggests that it performs slightly better in predicting VTEC during disturbed conditions compared to the other three ML models. The RMSE values of the stacked model range from 2.88 to 6.43 TECU, whereas the RMSE values of the IRI 2020 model range from 4.02 to 16.75 TECU. This indicates that the predictions made by the IRI 2020 model are poor compared to the ML models during geomagnetic disturbances at the specific location our study has focused on.

### 3.3 Seasonal Analysis

To compare the predictive performance of different models in predicting seasonal variations of VTEC, we used the 24-hour monthly average VTEC data for selected months

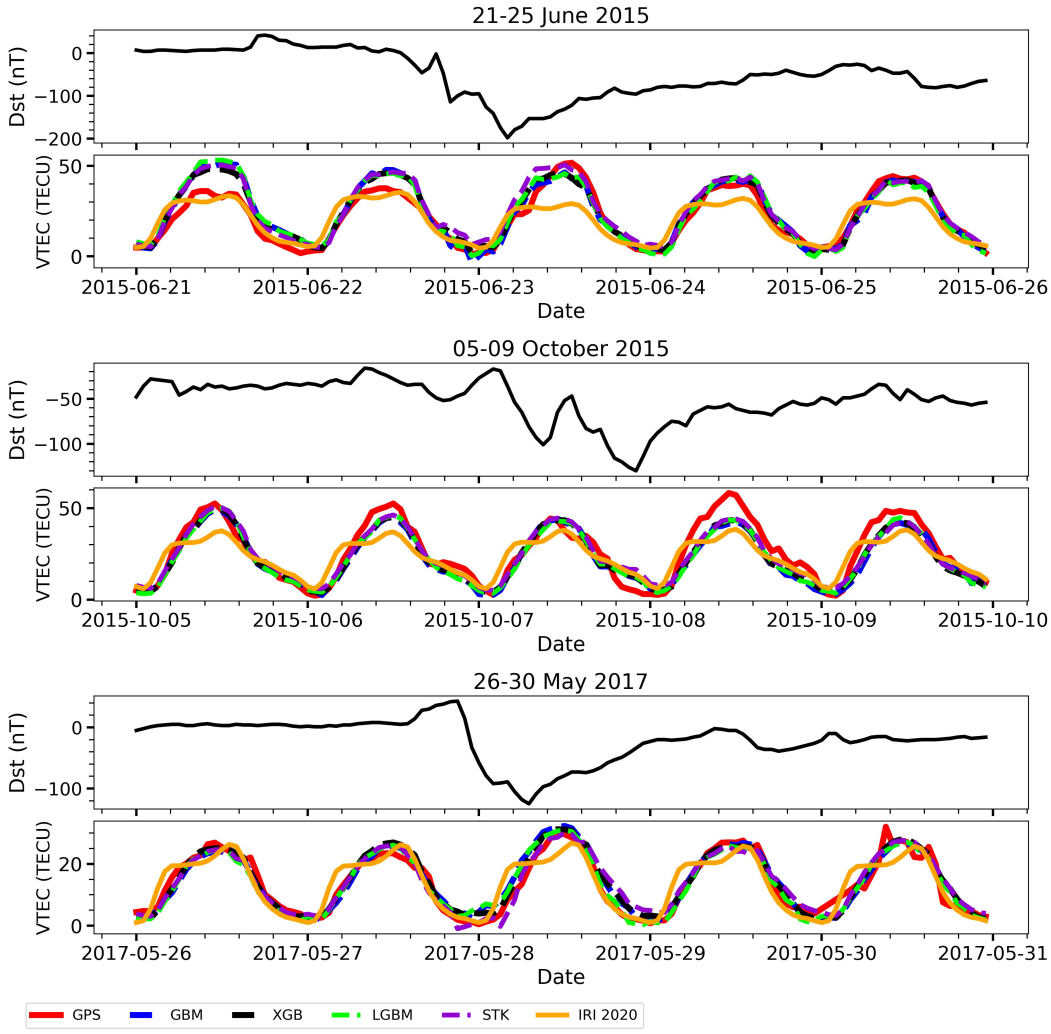


**Figure 6.** Plots of Dst index and comparison of predicted VTEC with the GPS VTEC for five-day periods with the day with intense storm considered at the center.

in various seasons as the testing data. In 2015, we selected March, June, September, and December, while March and June were selected in 2017. Figures 10 present the comparisons of 24-hour monthly mean variations of GPS VTEC and VTEC predicted by the GBM, XGBoost (XGB), LightGBM (LGBM), stacked (STK), and IRI 2020 models for the selected months. In the plots, GPS VTEC is represented by the red-colored line, while VTEC predicted by the models is represented by the blue, black, lime, dark violet, and orange-colored lines, respectively. As shown in the plots, the ML models successfully predicted VTEC values that align with GPS VTEC. However, the IRI 2020 model predictions showed significant deviations from GPS VTEC during the selected months.

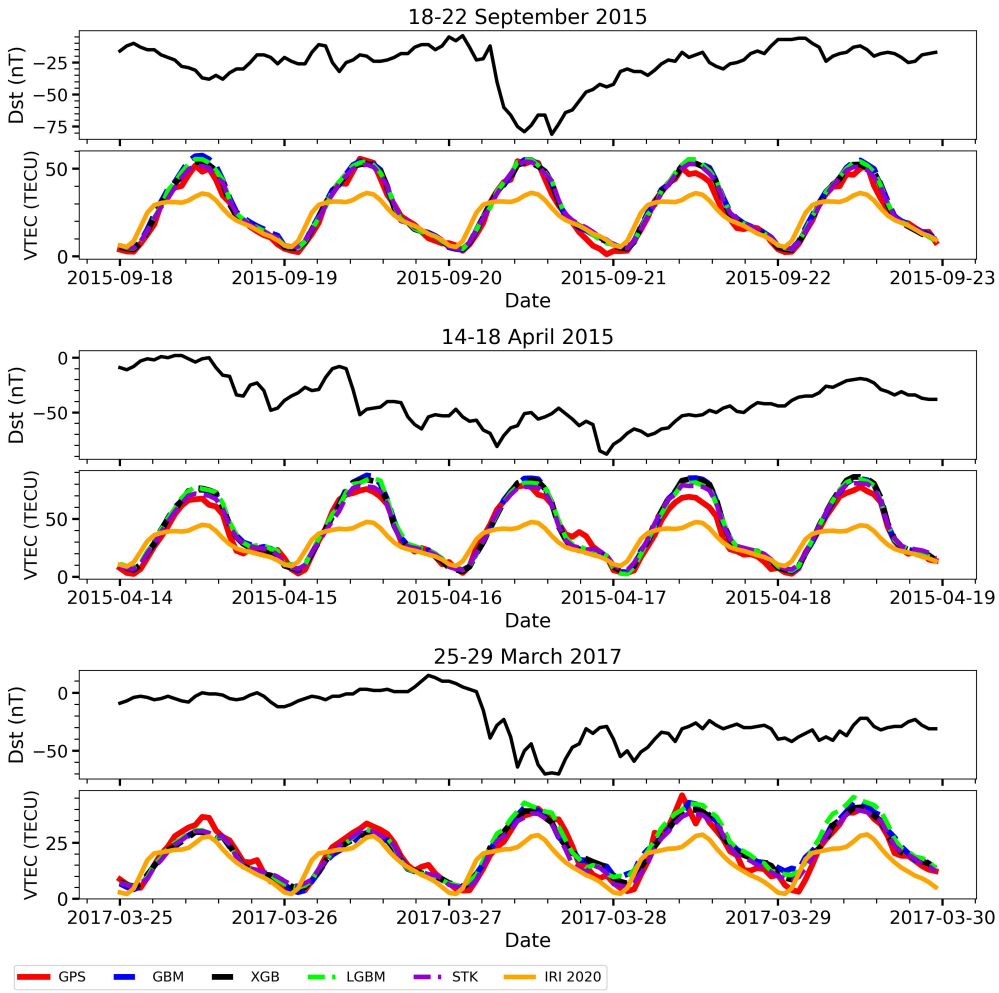


**Figure 7.** Plots of Dst index and comparison of predicted VTEC with the GPS VTEC for five-day periods with the day with moderate storm considered at the center.

The bar graph in Figure 11 displays the comparison of RMSE values for the machine learning (ML) models and the IRI 2020 model for the selected months on the testing data. The graph shows that the stacked model had lower RMSE values in March 2015, September 2015, and March 2017 when compared to other GBDT models. The XGBoost model exhibited a slightly lower RMSE value in June 2015 compared to other ML models. On the other hand, the GBM model had a slightly smaller RMSE value in June 2017. During the chosen months, the RMSE values for all models were higher in March 2015, which is due to the larger VTEC values during that month caused by it being closer to the solar maximum. The stacked model exhibited RMSE values ranging from 2.327 to 8.428 TECU, while the IRI 2020 model showcased RMSE values ranging from 4.085 to

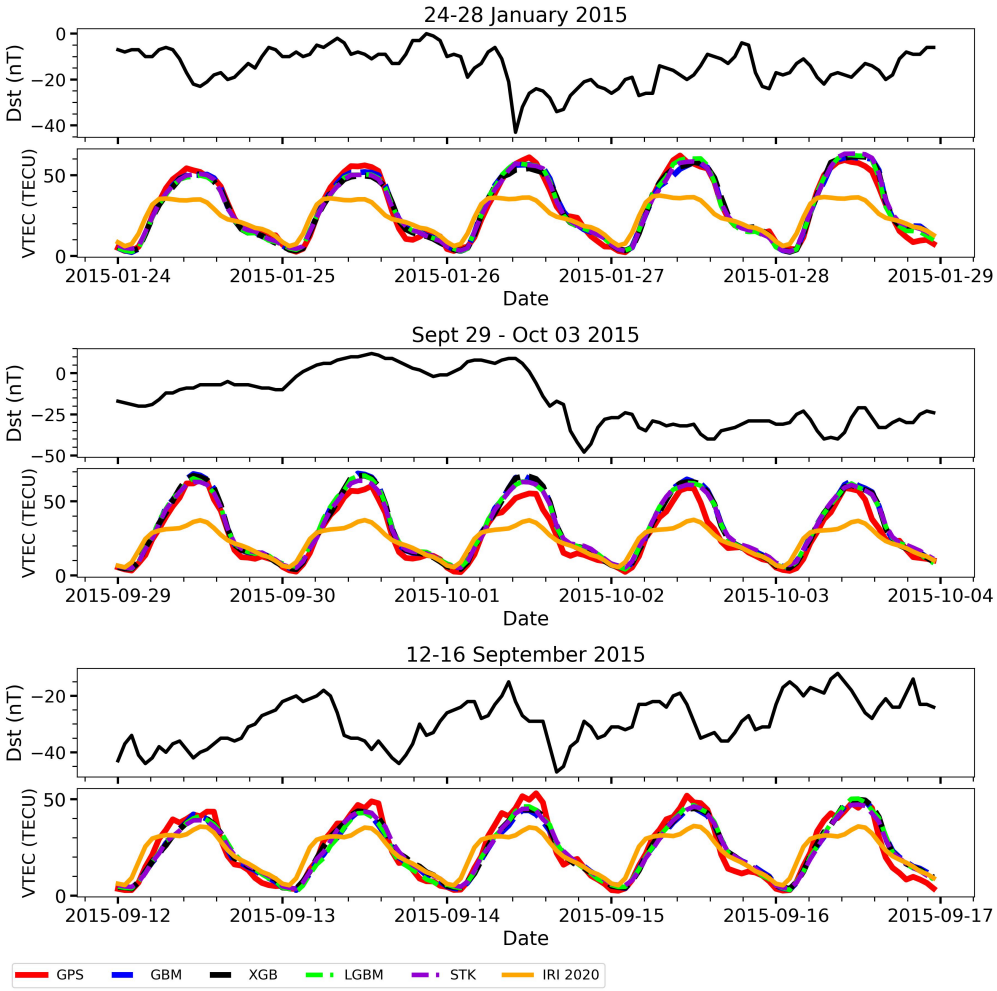


**Figure 8.** Plots of Dst index and comparison of predicted VTEC with the GPS VTEC for five-day periods with the day with weak storm considered at the center.

412 19.985 TECU. This indicates that the IRI 2020 model is less effective in predicting VTEC
413 compared to the ML models.

## 414 4 Conclusions

415 This paper compares the performance of four machine learning models for estimat-
416 ing ionospheric VTEC. The models used include GBM, XGBoost, Light-GBM, and a stacked
417 algorithm that combines the three models with a linear regression algorithm. A total of
418 8 years (2011–2018) of data was derived from the Addis Ababa GPS station in Ethiopia.
419 The data for years 2011–2014, 2016, 2018, and the second half of 2017 was utilized in
420 the development of the ML models. Testing was conducted on the dataset for 2015 and

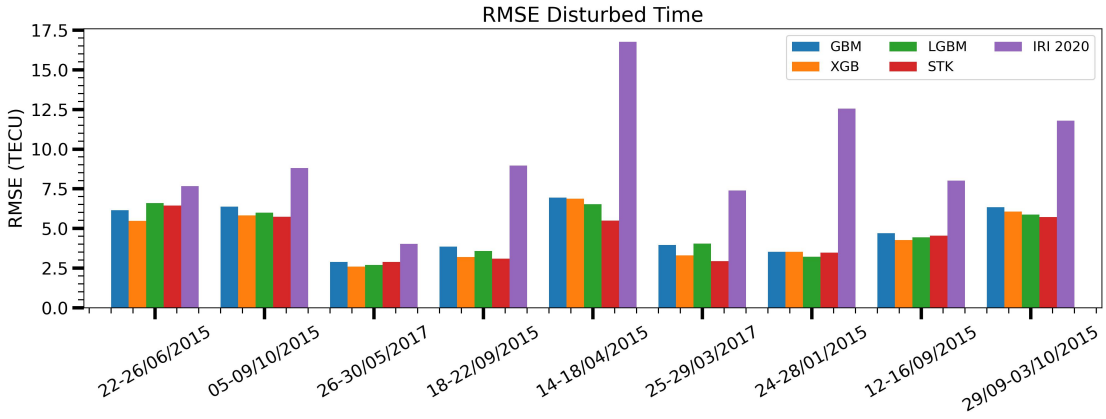


**Figure 9.** Comparison of the RMSE values of the machine learning models and IRI 2020 model for the periods considered to compare the performance of the models in geomagnetic disturbance.

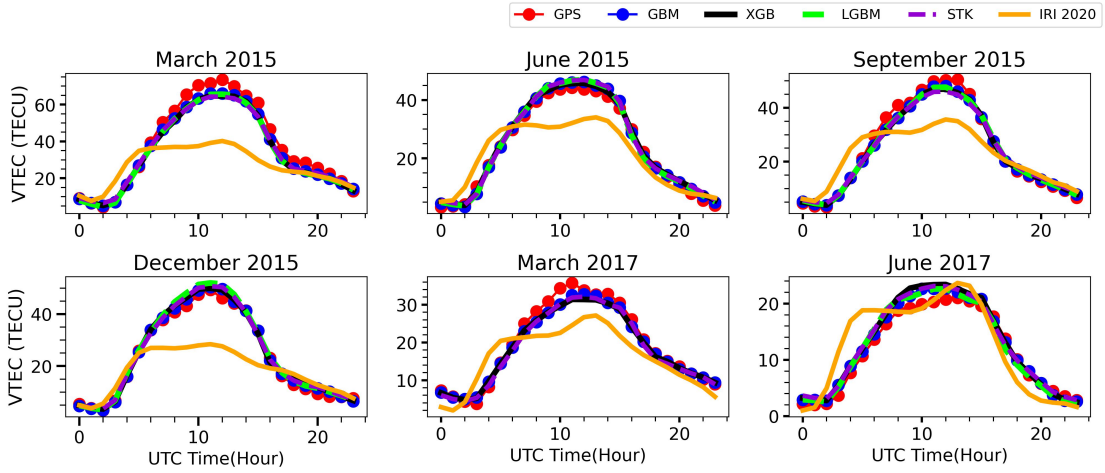


**Figure 10.** Comparison of seasonal variations of VTEC using the monthly 24 hour average VTEC of the models with the GPS VTEC for selected months in 2015 and 2017.

the first six months of 2017. In developing and testing models, the ML input data includes factors affecting VTEC variation such as time of day, season, solar and geomagnetic activity, and solar wind. The RandomizedSearchCV algorithm was used to determine the optimal hyperparameters of the models. A comparative analysis was conducted to validate the performance of machine learning models against the global model. The correlation between GPS VTEC and predicted VTEC for the four machine learning models showed almost identical results, with an R value of approximately 0.96, while the global model had a correlation of 0.87.

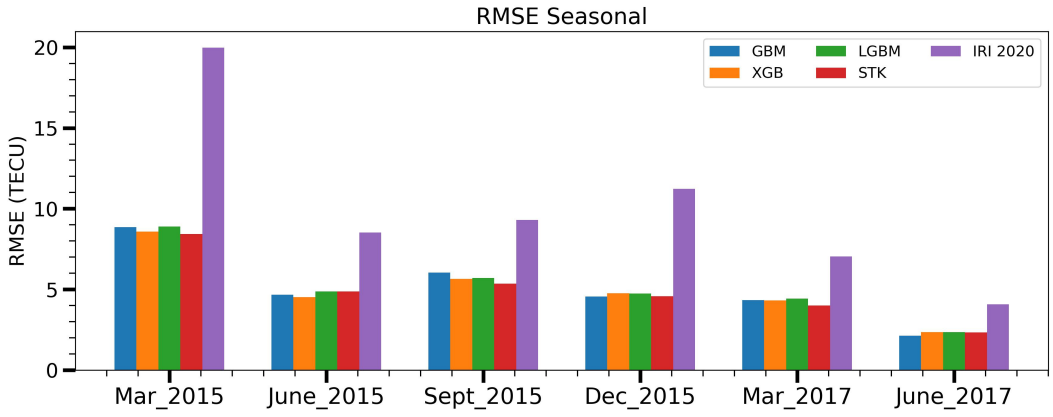


**Figure 11.** Comparison of RMSE values of the ML and IRI 2020 models for the selected months at different seasons in 2015 and 2017.

An error analysis between the model-predicted VTEC values and the GPS VTEC for the testing data showed that the ML models have significantly outperformed the IRI 2020 model in predicting VTEC. The VTEC predictions of the four ML and IRI 2020 models were compared with the GPS VTEC at selected quiet and geomagnetically disturbed conditions. The ML models have predicted VTEC with good accuracy and outperformed the IRI 2020 model in the selected quiet and disturbed conditions. The seasonal predictive performances of the models were also evaluated by comparing the 24-hour monthly average predicted VTEC values with the GPS VTEC for selected months at different seasons on the testing data. The VTEC values predicted by the ML models are in good agreement with the GPS VTEC, greatly outperforming the IRI 2020 model in the selected months with far smaller RMSE values. In general, the stacking algorithm applied in this study slightly reduced errors and slightly enhanced the predictive performance of the three gradient-boosting-based models in some instances. The findings in this study suggest that using GBDT algorithms and their stacked combination can accurately predict ionospheric VTEC in the African low-latitude region while also being computationally efficient.

## Data Availability Statement

The calibrated IGS TEC data for the Addis Ababa GPS receiver is available at the ICTP GNSS TEC calibration service (https://arplsrv.ictp.it/). Data corresponding to Amboo and Nazeret GPS receiver stations was obtained from the UNAVCO data archive

(https://www.unavco.org/data/gps-gnss). The data for the input variables sunspot number, solar radio flux F10.7, ap index, Dst index, solar wind plasma speed (SW), and Bz component of the IMF were downloaded from https://omniweb.gsfc.nasa.gov/form/dx1.html. The IRI 2020 model TEC data is available at https://kauai.ccmc.gsfc.nasa.gov/instantrun/iri/.

**Acknowledgments**

A. Tebabal's research is supported by the TWAS-DFG cooperation visits program and the Air Force Office of Scientific Research, United States, under award number FA8655-22-1-0001.

## References

Bentéjac, C., Csörgő, A., & Martínez-Muñoz, G. (2021). A comparative analysis of gradient boosting algorithms. *Artificial Intelligence Review*, *54*, 1937–1967. https://doi.org/10.1007/s10462-020-09896-5

Bilitza, D. (2001). International reference ionosphere 2000. *Radio Science*, *36*(2), 261-275. https://doi.org/10.1029/2000RS002432

Bilitza, D., Altadill, D., Truhlik, V., Shubin, V., Galkin, I., Reinisch, B., & Huang, X. (2017). International reference ionosphere 2016: From ionospheric climate to real-time weather predictions. *Space weather*, *15*(2), 418–429. https://doi.org/10.1002/2016SW001593

Bilitza, D., McKinnell, L.-A., Reinisch, B., & Fuller-Rowell, T. (2011). The international reference ionosphere today and in the future. *Journal of Geodesy*, *85*, 909–920. https://doi.org/10.1007/s00190-010-0427-x

Brownlee, J. (2016). *Xgboost with python: Gradient boosted trees with xgboost and scikit-learn*. Machine Learning Mastery.

Chen, T., & Guestrin, C. (2016). Xgboost: A scalable tree boosting system. Association for Computing Machinery. https://doi.org/10.1145/2939672.2939785

Ciraolo, L., Azpilicueta, F., Brunini, C., Meza, A., & Radicella, S. M. (2007). Calibration errors on experimental slant total electron content (tec) determined with gps. *Journal of geodesy*, *81*, 111–120. https://doi.org/10.1007/s00190-006-0093-1

Davies, K., & Hartmann, G. K. (1997). Studying the ionosphere with the global

positioning system. *Radio Science*, *32*(4), 1695-1703. https://doi.org/10.1029/97RS00451

Fafalios, S., Charonyktakis, P., & Tsamardinos, I. (2020). Gradient boosting trees. *Gnosis Data Analysis PC*, 1–3.

Habarulema, J. B., McKinnell, L.-A., & Cilliers, P. J. (2007). Prediction of global positioning system total electron content using neural networks over south africa. *Journal of Atmospheric and Solar-Terrestrial Physics*, *69*(15), 1842-1850. https://doi.org/10.1016/j.jastp.2007.09.002

Habarulema, J. B., McKinnell, L.-A., Cilliers, P. J., & Opperman, B. D. (2009). Application of neural networks to south african gps tec modelling. *Advances in Space Research*, *43*(11), 1711-1720. https://doi.org/10.1016/j.asr.2008.08.020

Habarulema, J. B., McKinnell, L.-A., & Opperman, B. D. (2011). Regional gps tec modeling; attempted spatial and temporal extrapolation of tec using neural networks. *Journal of geophysical research: space physics*, *116*(A4). https://doi.org/10.1029/2010JA016269

Habyarimana, V., Habarulema, J. B., & Mungufeni, P. (2020). On the possible contribution of ionospheric vertical drifts to tec modelling in low latitudes. *Advances in Space Research*, *65*(10), 2391-2404. https://doi.org/10.1016/j.asr.2020.02.005

Hajra, R., Chakraborty, S. K., Tsurutani, B. T., DasGupta, A., Echer, E., Brum, C. G., ... Sobral, J. H. A. (2016). An empirical model of ionospheric total electron content (tec) near the crest of the equatorial ionization anomaly (eia). *Journal of Space Weather and Space Climate*, *6*, A29. https://doi.org/10.1051/swsc/2016023

Han, Y., Wang, L., Fu, W., Zhou, H., Li, T., & Chen, R. (2021). Machine learning-based short-term gps tec forecasting during high solar activity and magnetic storm periods. *IEEE Journal of Selected Topics in Applied Earth Observations and Remote Sensing*, *15*, 115–126. https://doi.org/10.1109/JSTARS.2021.3132049

Hastie, T., Friedman, J., & Tibshirani, R. (2009). The elements of statistical learning: data mining, inference, and prediction. Springer New York. https://doi.org/10.1007/978-0-387-21606-5_2

He, Z., Lin, D., Lau, T., & Wu, M. (2019). Gradient boosting machine: a survey. *arXiv preprint arXiv:1908.06951*. https://doi.org/10.48550/arXiv.1908.06951

Hochegger, G., Nava, B., Radicella, S., & Leitinger, R. (2000). A family of ionospheric models for different uses. *Physics and Chemistry of the Earth, Part C: Solar, Terrestrial and Planetary Science*, *25*(4), 307-310. https://doi.org/10.1016/S1464-1917(00)00022-2

Ke, G., Meng, Q., Finley, T., Wang, T., Chen, W., Ma, W., ... Liu, T.-Y. (2017). Lightgbm: A highly efficient gradient boosting decision tree. *Advances in neural information processing systems*, *30*.

Klobuchar, J. A. (1996). Ionospheric effects on gps. *Chapter 12 of Global Positioning System: Theory and Applications*, *1*, 30.

Liu, L., Zou, S., Yao, Y., & Wang, Z. (2020). Forecasting global ionospheric tec using deep learning approach. *Space Weather*, *18*(11), e2020SW002501. https://doi.org/10.1029/2020SW002501

Lu, M., Hou, Q., Qin, S., Zhou, L., Hua, D., Wang, X., & Cheng, L. (2023). A stacking ensemble model of various machine learning models for daily runoff forecasting. *Water*, *15*(7), 1265. https://doi.org/10.3390/w15071265

Mannucci, A. J., Wilson, B. D., & Edwards, C. D. (1993). A new method for monitoring the earth's ionospheric total electron content using the gps global network. *Proceedings of ION GPS-93*, 22-24.

Maruyama, T. (2007). Regional reference total electron content model over japan based on neural network mapping techniques. *Annales Geophysicae*, *25*(12), 2609–2614. https://doi.org/10.5194/angeo-25-2609-2007

Natekin, A., & Knoll, A. (2013). Gradient boosting machines, a tutorial. *Frontiers in neurorobotics*, *7*, 21. https://doi.org/10.3389/fnbot.2013.00021

Natras, R., Soja, B., & Schmidt, M. (2022). Ensemble machine learning of random forest, adaboost and xgboost for vertical total electron content forecasting. *Remote Sensing*, *14*(15). https://doi.org/10.3390/rs14153547

Nava, B., Coïsson, P., & Radicella, S. (2008). A new version of the nequick ionosphere electron density model. *Journal of Atmospheric and Solar-Terrestrial Physics*, *70*(15), 1856-1862. https://doi.org/10.1016/j.jastp.2008.01.015

Nigussie, M., Radicella, S., Damtie, B., Nava, B., Yizengaw, E., & Groves, K. (2013). Validation of the nequick 2 and iri-2007 models in east-african equatorial region. *Journal of Atmospheric and Solar-Terrestrial Physics*, *102*, 26-33. https://doi.org/10.1016/j.jastp.2013.04.016

Okoh, D., Onwuneme, S., Seemala, G., Jin, S., Rabiu, B., Nava, B., & Uwamahoro, J. (2018). Assessment of the nequick-2 and iri-plas 2017 models using global and long-term gnss measurements. *Journal of Atmospheric and Solar-Terrestrial Physics*, *170*, 1-10. https://doi.org/10.1016/j.jastp.2018.02.006

Okoh, D., Owolabi, O., Ekechukwu, C., Folarin, O., Arhiwo, G., Agbo, J., ... Rabiu, B. (2016). A regional gnss-vtec model over nigeria using neural networks: A novel approach. *Geodesy and Geodynamics*, *7*(1), 19-31. https://doi.org/10.1016/j.geog.2016.03.003

Rahmadayana, F., Sibaroni, Y., et al. (2021). Sentiment analysis of work from home activity using svm with randomized search optimization. *Jurnal RESTI (Rekayasa Sistem dan Teknologi Informasi)*, *5*(5), 936–942. https://doi.org/10.29207/resti.v5i5.3457

Rama Rao, P. V. S., Niranjan, K., Prasad, D. S. V. V. D., Gopi Krishna, S., & Uma, G. (2006). On the validity of the ionospheric pierce point (ipp) altitude of 350 km in the indian equatorial and low-latitude sector. *Annales Geophysicae*, *24*(8), 2159–2168. https://doi.org/10.5194/angeo-24-2159-2006

Rokach, L., & Maimon, O. (2005). Decision trees. *Data mining and knowledge discovery handbook*, 165–192. https://doi.org/10.1007/0-387-25465-X_9

Sagi, O., & Rokach, L. (2018). Ensemble learning: A survey. *Wiley Interdisciplinary Reviews: Data Mining and Knowledge Discovery*, *8*(4), e1249. https://doi.org/10.1002/widm.1249

Shi, S., Zhang, K., Wu, S., Shi, J., Hu, A., Wu, H., & Li, Y. (2022). An investigation of ionospheric tec prediction maps over china using bidirectional long short-term memory method. *Space Weather*, *20*(6), e2022SW003103. https://doi.org/10.1029/2022SW003103

Tang, J., Li, Y., Ding, M., Liu, H., Yang, D., & Wu, X. (2022). An ionospheric tec forecasting model based on a cnn-lstm-attention mechanism neural network. *Remote Sensing*, *14*(10), 2433. https://doi.org/10.3390/rs14102433

Tebabal, A., Radicella, S., Damtie, B., Migoya-Orue', Y., Nigussie, M., & Nava, B. (2019). Feed forward neural network based ionospheric model for the east african region. *Journal of Atmospheric and Solar-Terrestrial Physics*, *191*, 105052. https://doi.org/10.1016/j.jastp.2019.05.016

Tebabal, A., Radicella, S., Nigussie, M., Damtie, B., Nava, B., & Yizengaw, E. (2018). Local tec modelling and forecasting using neural networks. *Journal of Atmospheric and Solar-Terrestrial Physics*, *172*, 143-151. https://doi.org/10.1016/j.jastp.2018.03.004

Xiong, P., Zhai, D., Long, C., Zhou, H., Zhang, X., & Shen, X. (2021). Long short-term memory neural network for ionospheric total electron content forecasting over china. *Space Weather*, *19*(4), e2020SW002706. https://doi.org/10.1029/2020SW002706

Yang, Y. (2017). Ensemble learning. *temporal data mining via unsupervised ensemble learning*, 35–56.

Zhou, Z.-H. (2021). *Machine learning*. Springer Nature. https://doi.org/10.1007/978-981-15-1967-3

Zhukov, A. V., Yasyukevich, Y. V., & Bykov, A. E. (2021). Gimli: Global ionospheric total electron content model based on machine learning. *GPS Solutions*, *25*(1), 1–9. https://doi.org/10.1007/s10291-020-01055-1

**Figure 1.**

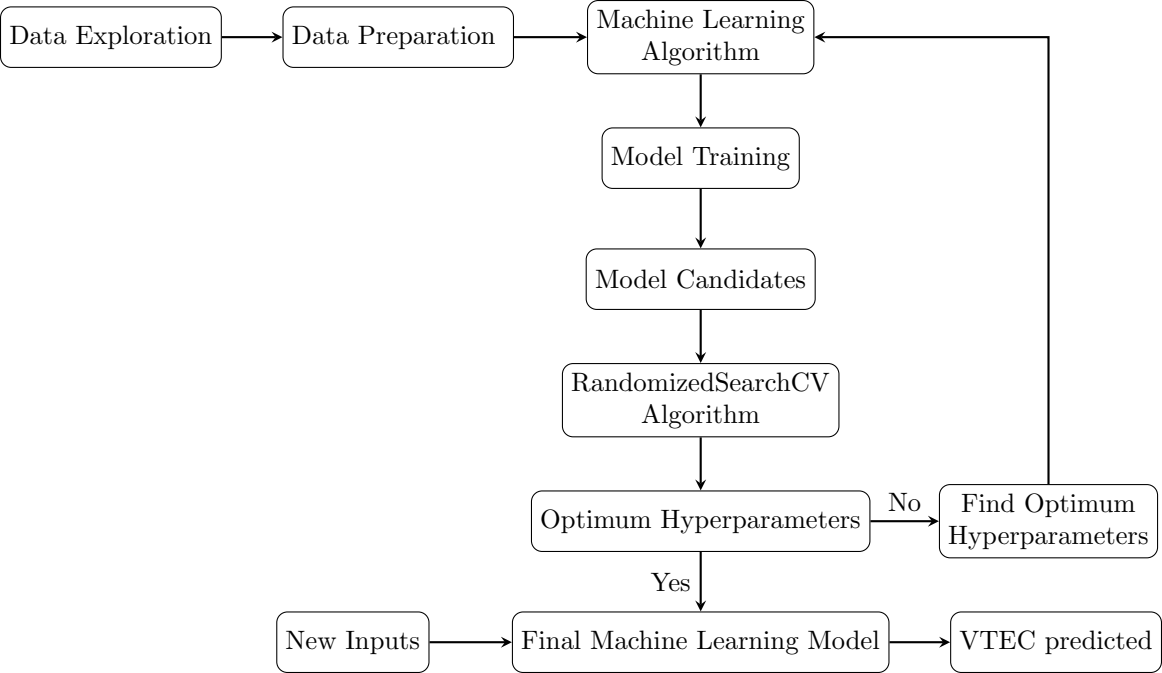
Data Exploration
Data Preparation
Machine Learning Algorithm
Model Training
Model Candidates
RandomizedSearchCV Algorithm
Optimum Hyperparameters
No
Find Optimum Hyperparameters
Yes
New Inputs
Final Machine Learning Model
VTEC predicted

**Figure 2.**

GBM

R = 0.960

$y = 0.904x + 1.690$

XGBoost

R = 0.961

$y = 0.892x + 1.875$

LightGBM

R = 0.960

$y = 0.913x + 1.417$

Stacked

R = 0.964

$y = 0.882x + 2.409$

Predicted VTEC (TECU)

GPS VTEC (TECU)

0 20 40 60 80

**Figure 3.**

GBM Error 2015

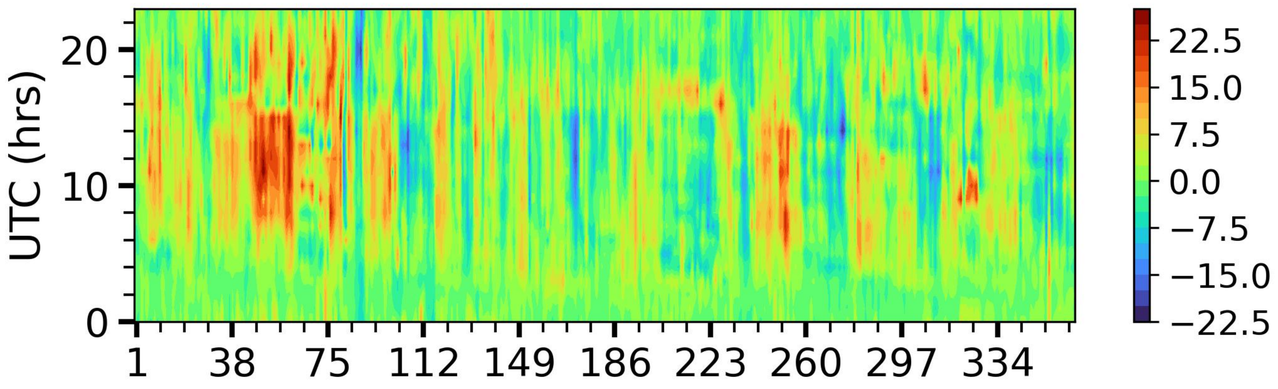


GBM Error 2017

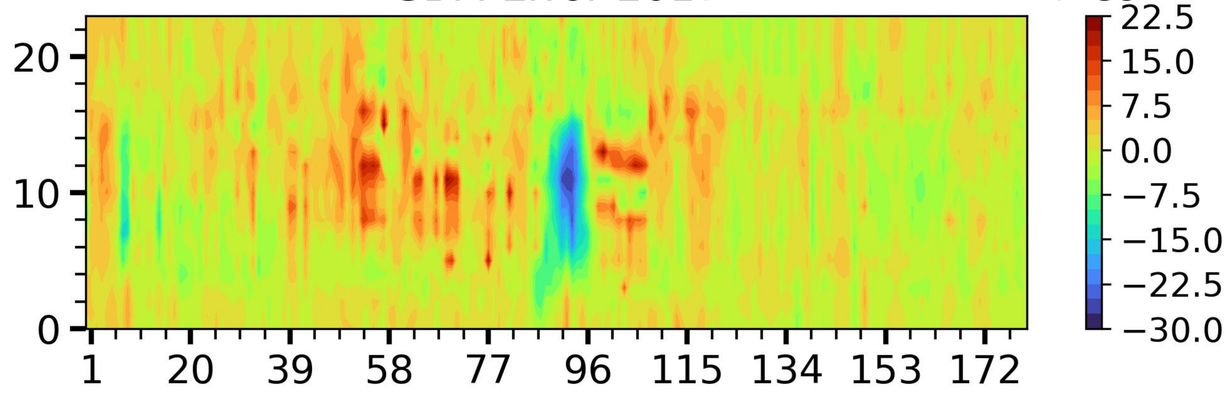


XGB Error 2015

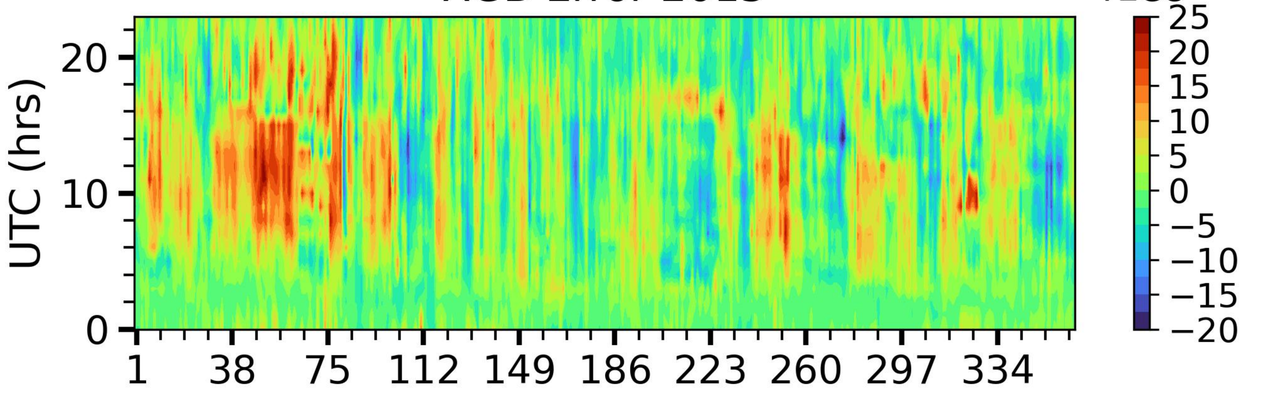


XGB Error 2017

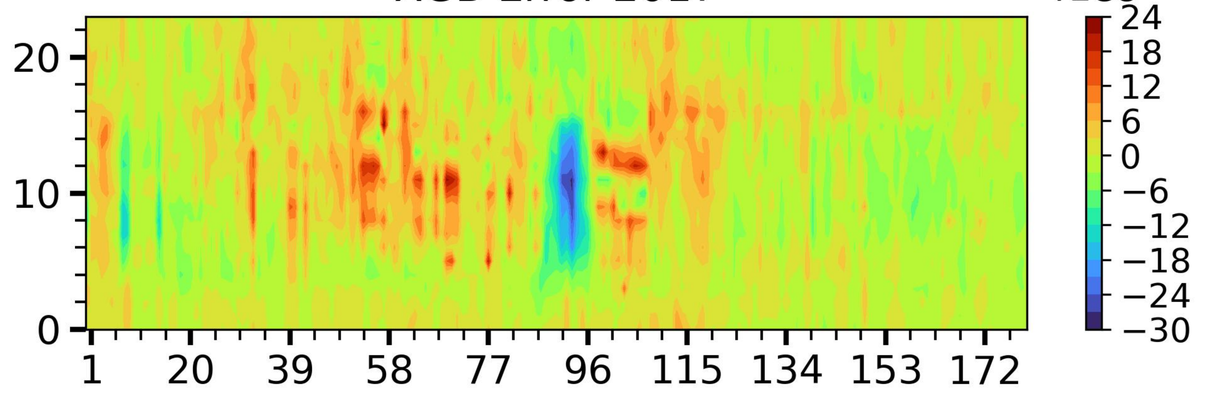


LGBM Error 2015

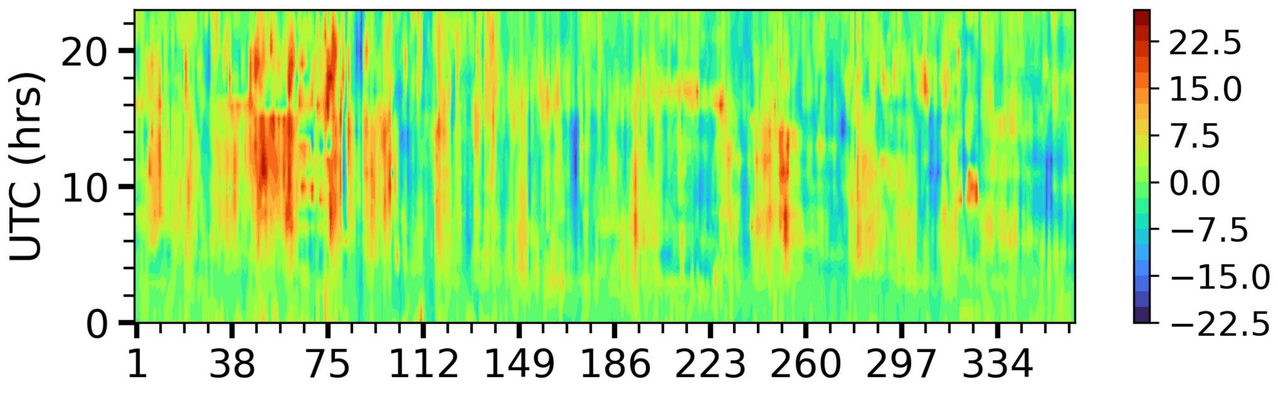


LGBM Error 2017

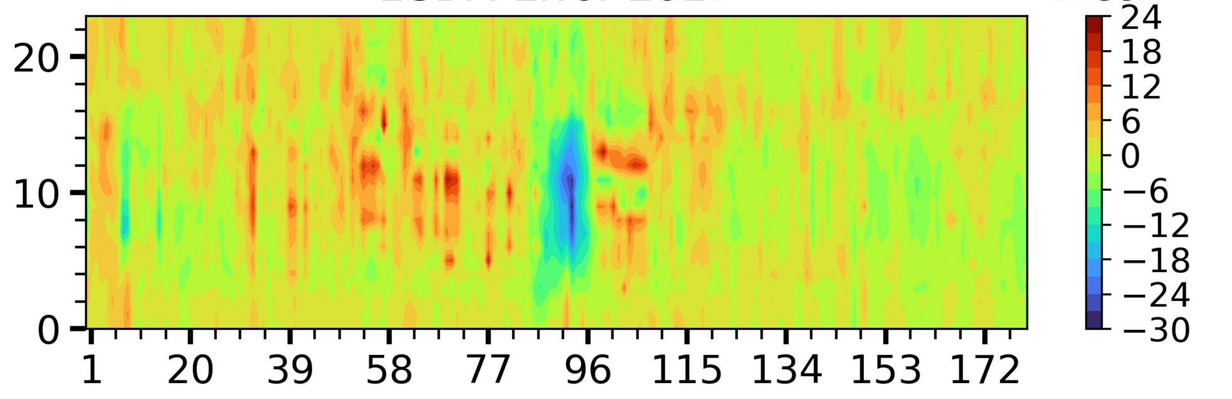


Stacked Error 2015

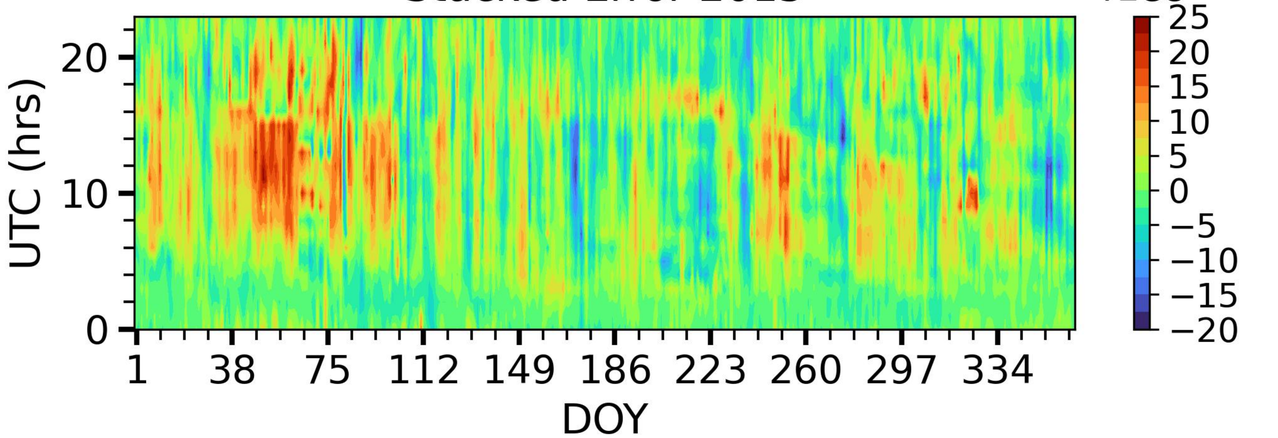


Stacked Error 2017

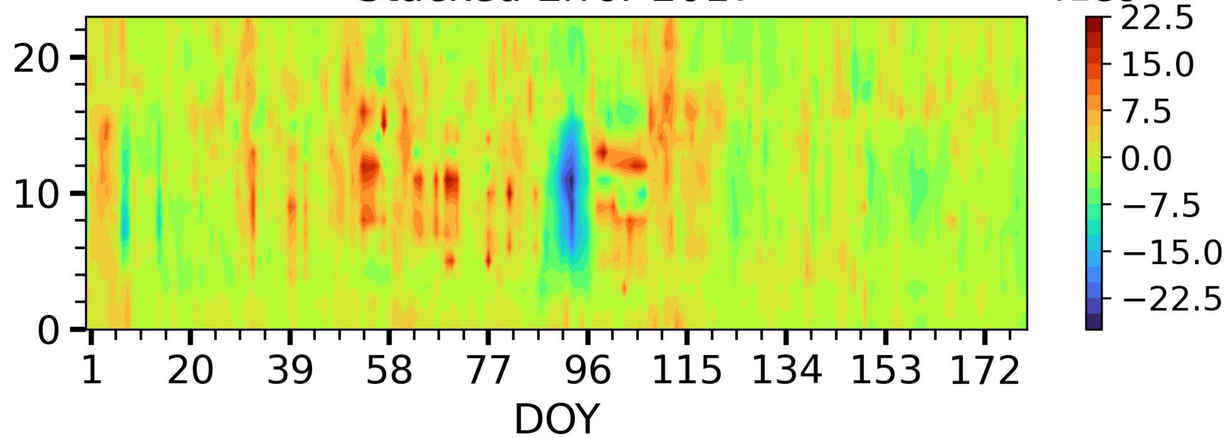

**Figure 4.**

GPS VTEC 2015

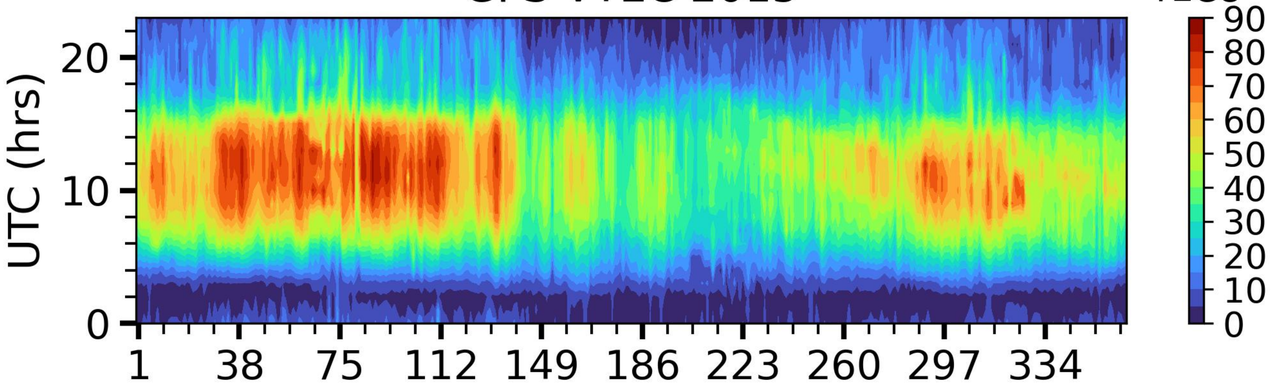


GPS VTEC 2017

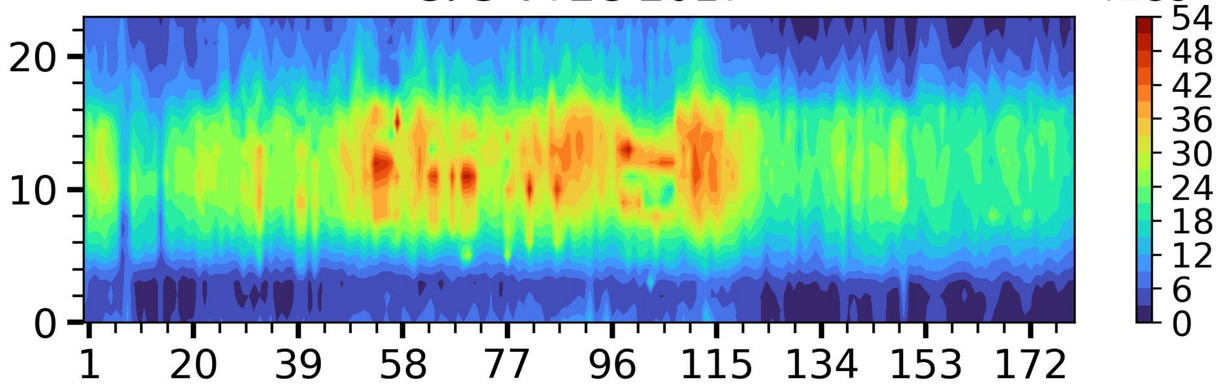


GBM VTEC 2015

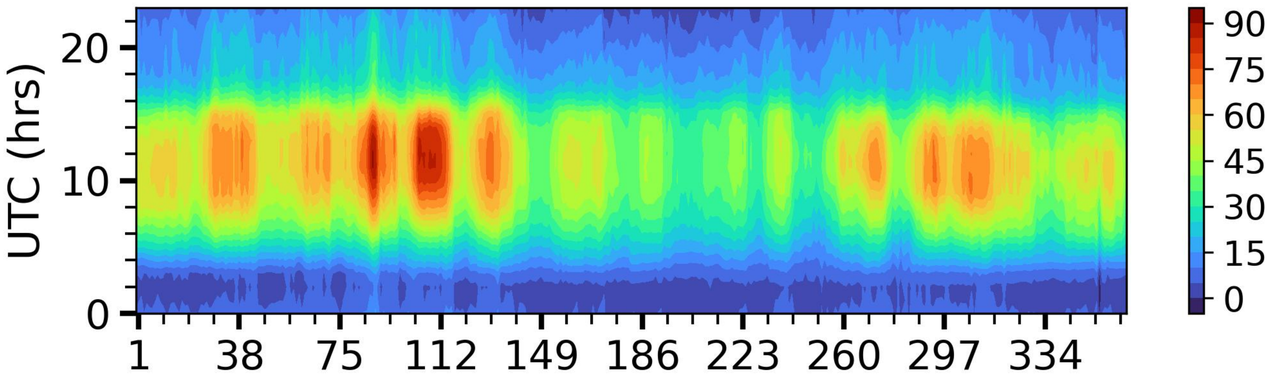


GBM VTEC 2017

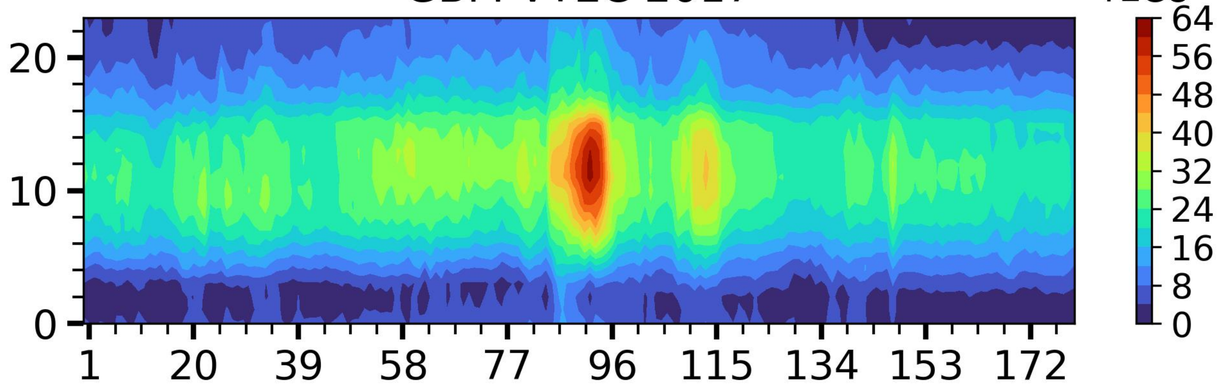


XGB VTEC 2015

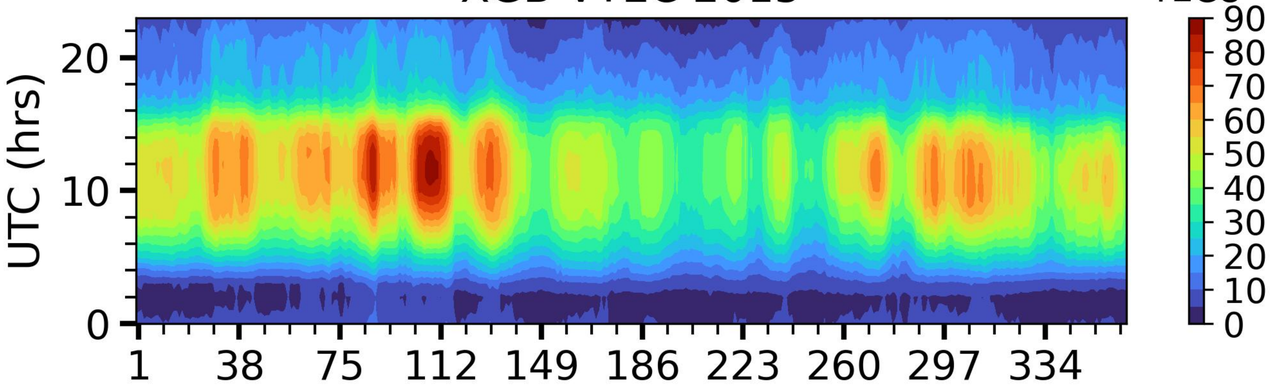


XGB VTEC 2017

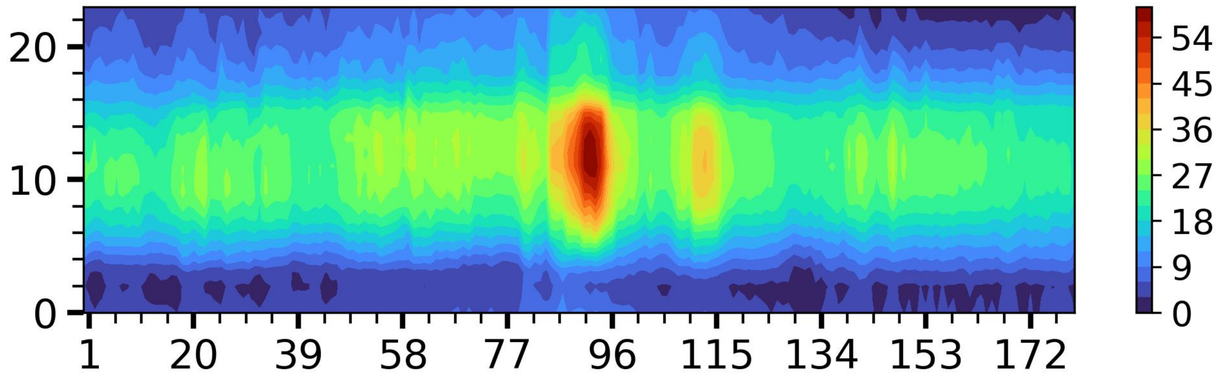


LGBM VTEC 2015

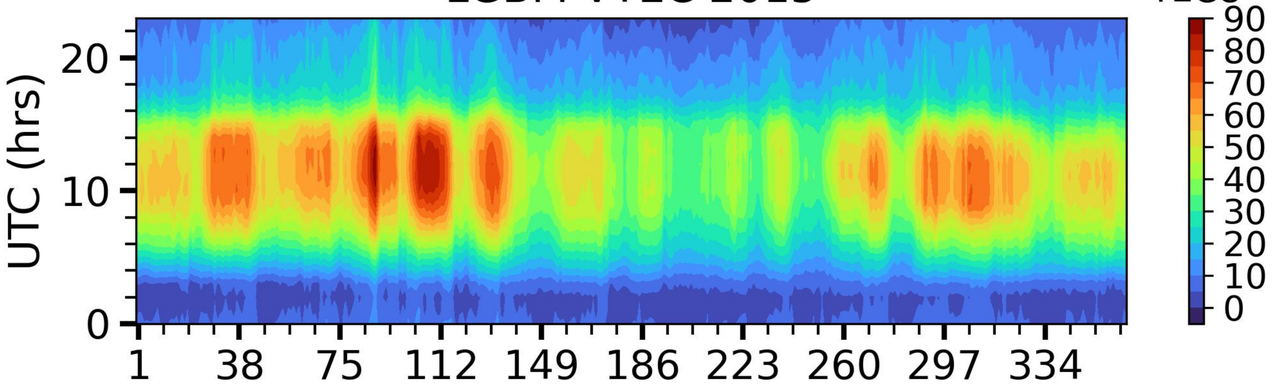


LGBM VTEC 2017

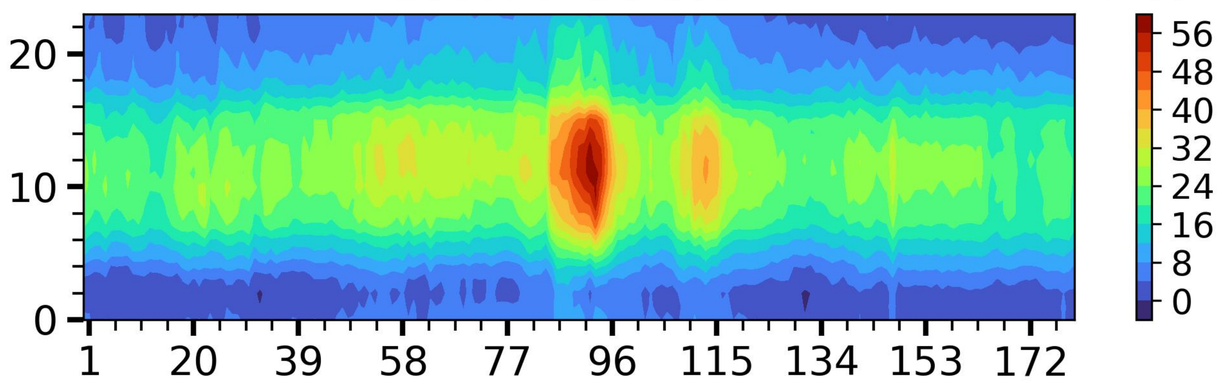


Stacked VTEC 2015

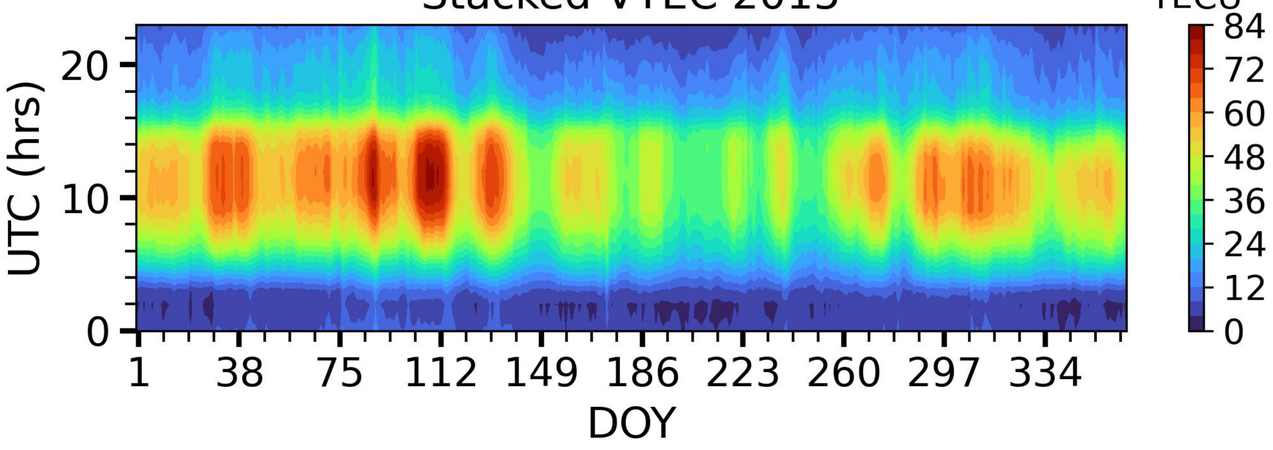


Stacked VTEC 2017

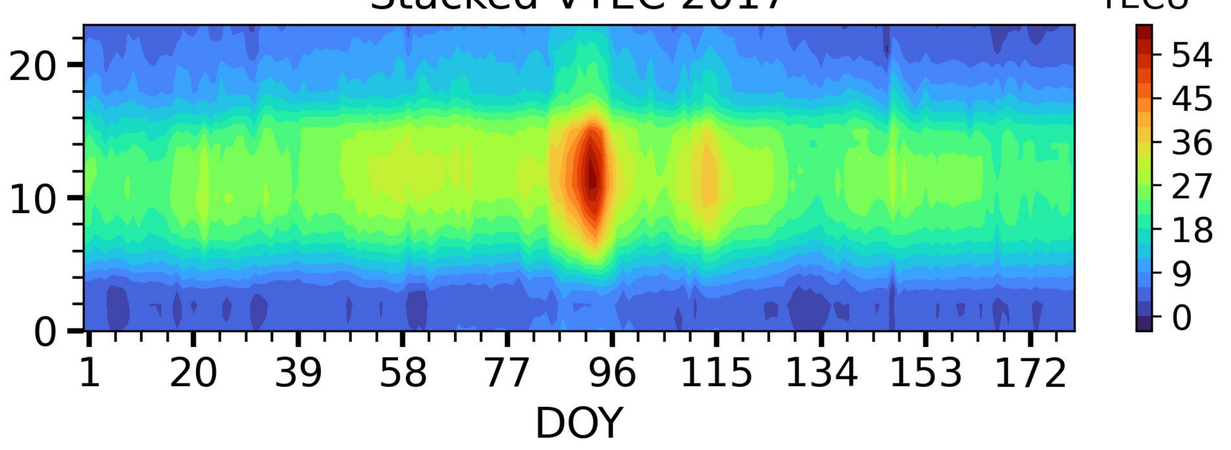

**Figure 5.**

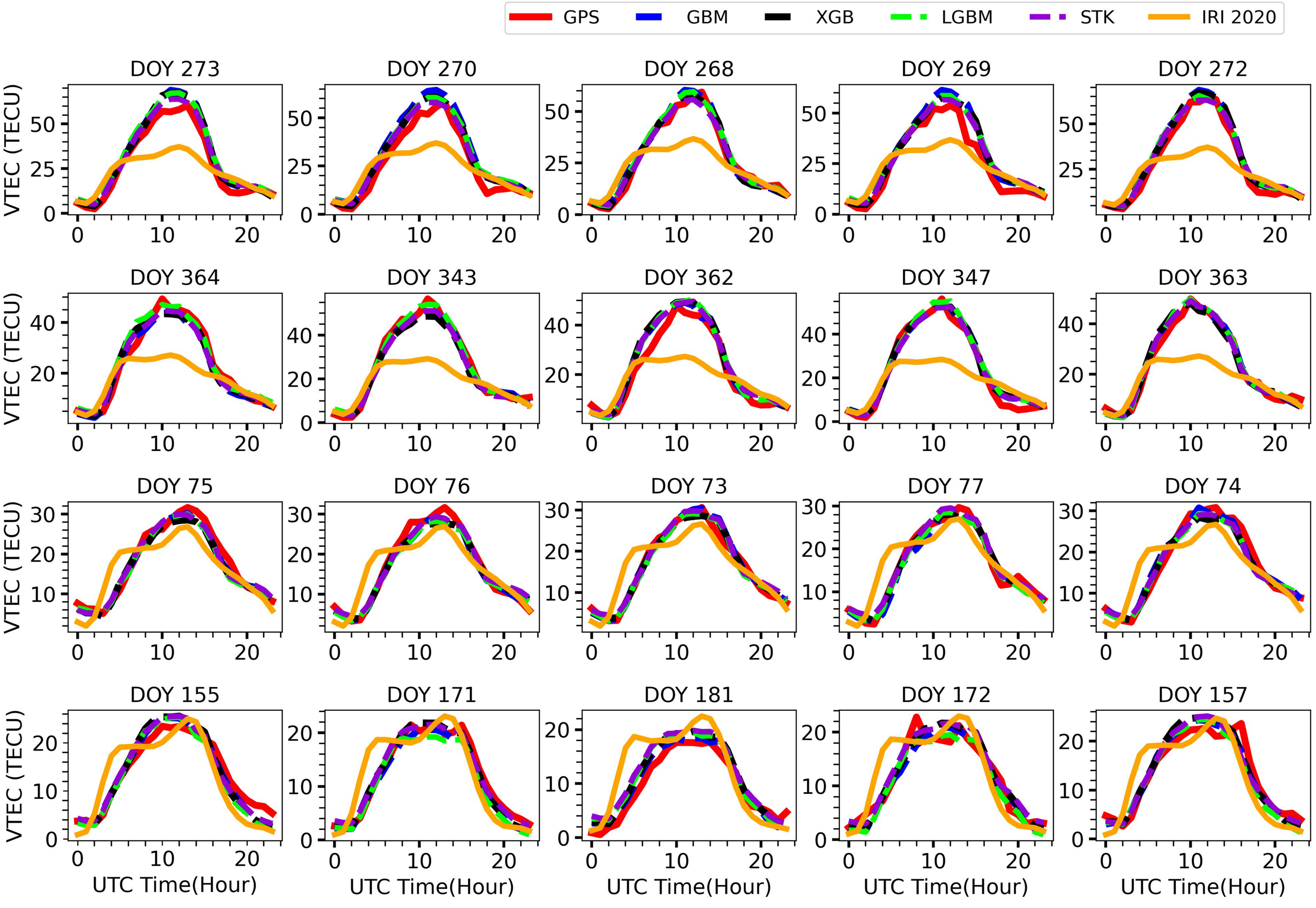
GPS
GBM
XGB
LGBM
STK
IRI 2020
DOY 273
DOY 270
DOY 268
DOY 269
DOY 272
DOY 364
DOY 343
DOY 362
DOY 347
DOY 363
DOY 75
DOY 76
DOY 73
DOY 77
DOY 74
DOY 155
DOY 171
DOY 181
DOY 172
DOY 157
VTEC (TECU)
UTC Time(Hour)

**Figure 6.**

21-25 June 2015

Dst (nT)

0
−100
−200

VTEC (TECU)

50
0

2015-06-21
2015-06-22
2015-06-23
2015-06-24
2015-06-25
2015-06-26

Date

05-09 October 2015

Dst (nT)

−50
−100

VTEC (TECU)

50
0

2015-10-05
2015-10-06
2015-10-07
2015-10-08
2015-10-09
2015-10-10

Date

26-30 May 2017

Dst (nT)

0
−100

VTEC (TECU)

20
0

2017-05-26
2017-05-27
2017-05-28
2017-05-29
2017-05-30
2017-05-31

Date

GPS
GBM
XGB
LGBM
STK
IRI 2020

**Figure 7.**

18-22 September 2015

Dst (nT)

−25
−50
−75

VTEC (TECU)

50
0

2015-09-18
2015-09-19
2015-09-20
2015-09-21
2015-09-22
2015-09-23

Date

14-18 April 2015

Dst (nT)

0
−50

VTEC (TECU)

50
0

2015-04-14
2015-04-15
2015-04-16
2015-04-17
2015-04-18
2015-04-19

Date

25-29 March 2017

Dst (nT)

0
−50

VTEC (TECU)

25
0

2017-03-25
2017-03-26
2017-03-27
2017-03-28
2017-03-29
2017-03-30

Date

GPS
GBM
XGB
LGBM
STK
IRI 2020

**Figure 8.**

24-28 January 2015

Dst (nT)

VTEC (TECU)

2015-01-24 2015-01-25 2015-01-26 2015-01-27 2015-01-28 2015-01-29

Date

Sept 29 - Oct 03 2015

Dst (nT)

VTEC (TECU)

2015-09-29 2015-09-30 2015-10-01 2015-10-02 2015-10-03 2015-10-04

Date

12-16 September 2015

Dst (nT)

VTEC (TECU)

2015-09-12 2015-09-13 2015-09-14 2015-09-15 2015-09-16 2015-09-17

Date

GPS GBM XGB LGBM STK IRI 2020

**Figure 9.**

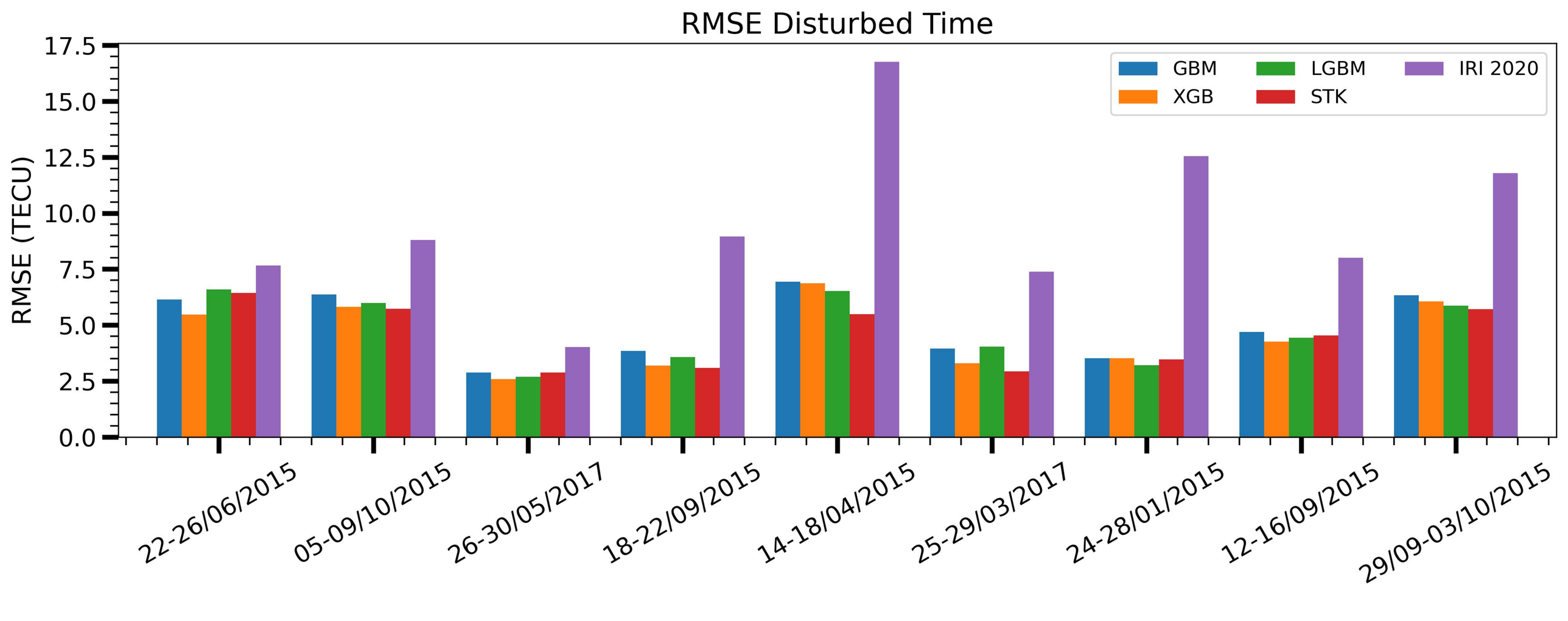
RMSE Disturbed Time
RMSE (TECU)
17.5
15.0
12.5
10.0
7.5
5.0
2.5
0.0
GBM
XGB
LGBM
STK
IRI 2020
22-26/06/2015
05-09/10/2015
26-30/05/2017
18-22/09/2015
14-18/04/2015
25-29/03/2017
24-28/01/2015
12-16/09/2015
29/09-03/10/2015

**Figure 10.**

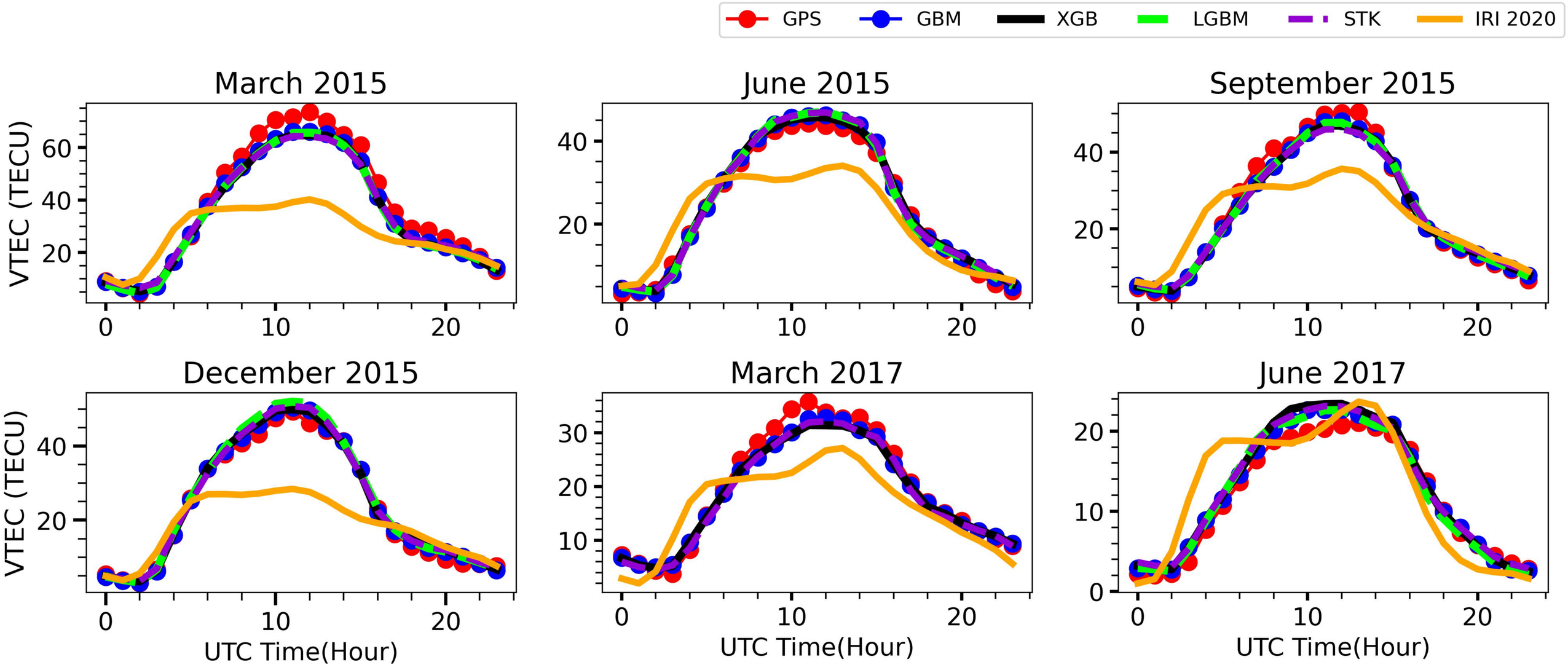
GPS
GBM
XGB
LGBM
STK
IRI 2020
March 2015
June 2015
September 2015
December 2015
March 2017
June 2017
VTEC (TECU)
VTEC (TECU)
UTC Time(Hour)
UTC Time(Hour)
UTC Time(Hour)

**Figure 11.**

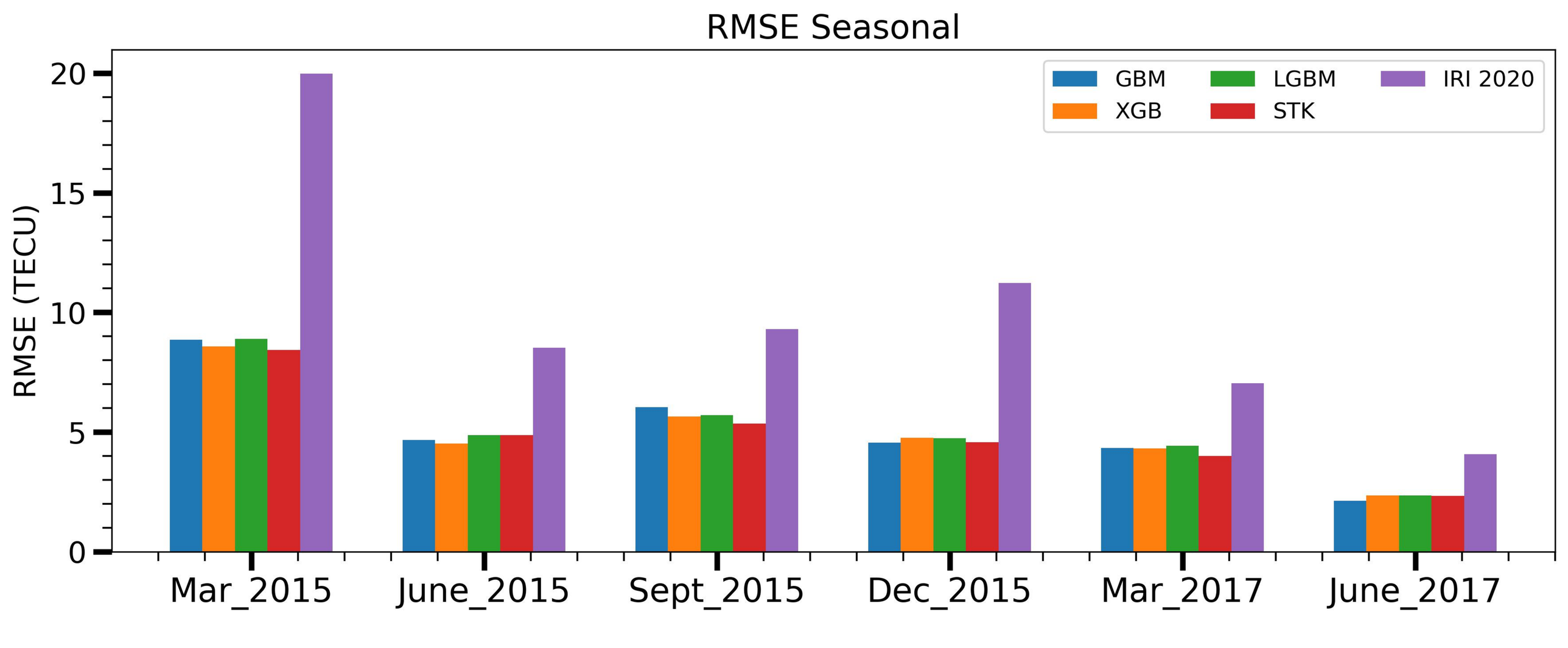
RMSE Seasonal
RMSE (TECU)
0
5
10
15
20
GBM
XGB
LGBM
STK
IRI 2020
Mar_2015
June_2015
Sept_2015
Dec_2015
Mar_2017
June_2017